3 Data and exploratory analysis

3.1 Introduction

This Chapter partially addresses both the 'pattern' (spatial and temporal) and 'cause' themes of this thesis. To test the hypotheses presented at the end of Chapter 2, the majority of climate phenomena presented in Sections 2.2, 2.3, and 2.4 must be quantified or represented. In this chapter the relevant data are introduced and tested for statistically significant relationships, along with temporal and spatial trends, prior to the modelling process (Chapter 4). Modelling is utilised as the main tool of this thesis, for the study of potentially causative behaviour and spatial differences in relationships. The exploratory analysis presented in this chapter is an important step in understanding the patterns of extreme climate and their physical causes, and therefore for ensuring that model predictors are selected based upon that understanding, rather than a purely statistical methodology.

Section 3.2 describes the climate data utilised throughout Chapters 3 and 4- daily data derived from weather stations across the Mediterranean region (3.2.1), and gridded pressure and specific humidity data-series (reanalysed) by NCEP/NCAR (Kalnay *et al.*, 1996) (3.2.2). Mathematical methods applied to climate data are detailed in Section 3.3. Section 3.4 then describes the procedures by which climate station data are processed to acquire indices representative of specific climate behaviour as identified in Chapter 2, followed by a description of their spatial distribution (3.4.2), inter-correlation (3.4.3), and trend (3.4.4) behaviour, summarised in Section 3.4.5. The factors that may influence indices of extreme behaviour are then discussed in Section 3.5. Section 3.5.1 describes properties desirable in predictors. Sections 3.5.2, 3.5.3, and 3.5.4 then quantifies the circulatory oscillations and indices discussed in Chapter 2.2.3, and analyses them for inter-correlation and trend behaviour. Sections 3.5.5, 3.5.6 and 3.5.7 describe the same procedure concerning the variance of localised climatology (sea level pressure, geopotential height, and specific humidity) discussed in Chapter 2.3.1. These two forms of predictor variable are then analysed for inter-correlation (3.5.8) and

tested against the predictands formed earlier in the Chapter (3.6). Section 3.7 collects findings novel to this chapter in preparation for Chapter 4.

3.2 Climate data sets

3.2.1 Mediterranean station data

This study focuses on extremes of climate that can be defined in terms of temperature or precipitation (flood, drought, heatwaves, cold snaps), and therefore requires daily data for maximum temperature (Tmax), minimum temperature (Tmin), mean temperature (Tmean), and total precipitation (Prec) over a given time period. When attempting to capture extremes of climate, certain constraints are placed upon the type of data that can be used (Karl *et al.*, 1999; Nicholls and Murray, 1999). Extreme events cannot be adequately characterised by gridded climate data as the spatial averaging process effectively reduces the magnitude of events (Frich *et al.*, 2002). Similarly so for temporally averaged data: it is therefore necessary to utilise daily data from point sources (Piñol *et al.*, 1998; Jones *et al.*, 1999a; Brunetti *et al.*, 2001b; Frich *et al.*, 2002; Yan *et al.*, 2002). Furthermore, to accurately define meaningful extreme events, climate data must be available for a period on the scale of decades (Karl *et al.*, 1999; Nicholls and Murray, 1999; Frich *et al.*, 2002). It is also important that each series under consideration possesses a complete or near complete set of high quality records over the period (Manton *et al.*, 2001). This causes problems when attempting to obtain data from the Balkans region of the Mediterranean, much of which has suffered civil unrest during recent years, or from Northern Africa. However, high quality data ensures that any apparent statistical relationship or trend is appropriate for the majority of the study period, and that the possibility of missing a particular extreme event is reduced (Manton *et al.*, 2001).

In this study, data from over 120 stations across the Mediterranean (35°-45°N, −10°-30°E) were acquired for the 1958-2000 period (as in Haylock and Goodess, 2004), which includes the 1961-1990 standard reference period (Manton *et al.*, 2001). The majority of these station records were compiled by the Spanish Fundación para la

Investigación del Clima (FIC), as part of the Statistical and Regional dynamical Downscaling of EXtremes for European regions (STARDEX) project, and largely supplied to the FIC by the Royal Netherlands Meteorological Institute (KNMI) (Klein-Tank *et al.*, 2002). Other bodies including the World Meteorological Office (WMO) and national meteorological services from Bosnia and Slovenia have also donated weather station data for this study. However, when conducting analysis of climate time series, data homogeneity must be considered (Alexandersson and Moberg, 1997; Jones *et al.*, 1999a; Karl *et al.*, 1999; Nichols and Murray, 1999; Manton *et al.*, 2001), and some stations have been rejected due to inhomogeneities. For more detail concerning climate data homogeneity and the tests performed in this study, see Section 3.3.1.

3.2.2 NCEP/NCAR reanalysis data

The term 'reanalysis' refers to a methodology that assimilates data from a large number of sources (e.g. land, ship, rawinsonde, aircraft, and satellite observations) into a single consistent model through time (even though data availability may change with time). At NCEP/NCAR incoming data undergoes four distinct stages to test for reliability (Kalnay *et al.*, 1996). Preprocessing compares input with pre-existing climatologies via tendency checks, homogeneity testing, box averages, and variance analysis. Parallel processing tests the assimilation of a new data source by processing a single year of data with and without the data source. The third stage is internal validation and is the most complex part of the validation process. Tests vary with data type but are often interpolative in nature. Through a combination of horizontal, vertical, hydrostatic and increment interpolation checks, a baseline elevation check and a temporal interpolation check, forecast and mean variables (such as sea level pressure, wind speed, and temperature), and errors in station locations, along with possible changes of location, may be obtained. This kind of quality control is known as 'optimal interpolation' (Woolen, 1991; Reid *et al.*, 2001). Finally the reanalysis system undergoes rigorous (but largely automated) monitoring. In its entirety, the process is computationally intensive, and takes time for input data to be gathered and collated. Output is thus retrospective. The end result of the reanalysis process is consistent and gridded data (NCEP/NCAR is currently at 2.5 by 2.5 degree resolution) for over 50

years, at multiple heights, for a very large number of variables (Kalnay *et al.*, 1996).

The NCEP/NCAR data were chosen over alternatives because at the beginning of this study they were unique in terms of coverage, both spatially and temporally. The closest comparable data set, the European Centre for Medium-range Weather Forecasts (ECMWF) Re-analysis Data Archive (ERA), has only recently progressed from 15 years of data (ERA-15) to 40 (ERA-40). By comparison, the NCEP/NCAR re-analyses covered a period from 1947-2001 at the beginning of this study (mid-2003), and as of late 2005 included daily data within weeks of its acquisition. A number of fairly substantial errors in the dataset have been highlighted by Kistler *et al.* (2001) but pressure and humidity data remain some of the most robust data, rating an A (strongly influenced by observed data, e.g. upper air temperature, and wind) or a B (strongly influenced by observed data and the reanalysis model, e.g. humidity, and surface temperature) rather than the C (derived entirely from model fields, e.g. clouds, and precipitation) rating applied to the majority of surface fluxes, not used in this study (Kalnay *et al.*, 1996). Reid *et al.* (2001) found that values for mean sea level pressure, a variable that is used in this study, are reliable on the interannual time scale, although more so for periods after 1967 and for low lying regions. Differences between UKMO recorded SLP and NCEP reanalyzed SLP are generally small (less than 2hPa) and the least reliable (differences up to 8 hPa) areas (over Greenland and the Barents Sea) are outside the domain of this study.

Over Europe the reanalysis data set is of 'research quality' in terms of both interannual and (less so) decadal variability, and is suitable for the purposes of this study, as for others (e.g. Quadrelli *et al.*, 2001; Bordi and Sutera, 2002; Goodess and Jones, 2002). In this study, the NCEP/NCAR reanalysis data set (Kalnay *et al.*, 1996) is utilised to construct synoptic-scale circulation indices from daily grids SLP and Z500 (geopotential height at the 500hPa level, Section 2.3.1). Constructed indices (section 2.2.3) include those for the Mediterranean Oscillation (Piervitalli *et al.*, 1999; Palutikof *et al.*, 2003), the North Atlantic Oscillation (Jones *et al.* 1997), and the El Nino Southern Oscillation (Ropelewski and Halpert, 1987). Although these latter phenomena already have reliable and well used indices, new interpolated indices were generated in order to ensure a consistent methodology and to allow for the potential generation of indices for future periods. This allows future work to construct projections of climate

behaviour from global climate models (Chapter 8). Reanalysis data were also used in this study to construct areal average indices (Section 3.5.2) and measures of spatial variance for sea level pressure, z500 heights, and specific humidity, as described in Section 3.3.7.

3.3 Analysis methodology

In this study a number of different statistical techniques are applied to the data detailed above for the purposes of data pre-processing (e.g. interpolation) and analysis (e.g. correlation and trend analysis). All climate stations undergo homogeneity testing, NCEP/NCAR data is subject to both interpolation (for the construction of circulation indices) and principal component analysis (for study and the construction of PCA indices), and indices of extremes, circulation, and field variance (see below) are tested for correlation and trend behaviour. The methods and equations associated with the relevant techniques are detailed below.

3.3.1 Homogeneity testing

Homogeneity refers to the consistency of a data set and the extent to which a data set varies only by that which it is supposed to represent, in this case, weather and climate (Conrad and Pollak, 1950). As weather stations are partially dependent upon their human operators, many different events may occur to render them temporally inconsistent (Manton *et al*., 2001). There may be changes in procedure or instrumentation, or stations may move from one position to another (Manton *et al*., 2001; Wijngaard *et al*., 2003). Information regarding these changes should be apparent within station metadata (additional information that describes the climate data) but it is sometimes difficult to interpret or even acquire good metadata (Peterson *et al*., 1998). Where metadata is lacking, techniques have been developed to detect and adjust for data homogeneity. Sudden jumps in monthly or seasonally calculated mean values, or the presence of significant numbers of statistically unlikely outliers may cause a station to become suspect (Peterson *et al*., 1998). Data can then be adjusted to realign mean

values, or to remove given outliers. Most of the homogenisation literature only details adjustments to monthly or seasonal data, as corrections required for daily data are much more complex (Jones *et al.*, 1999a; Wjingaard *et al.*, 2003).

Gonzalez-Rouco *et al.* (2001) describe quality control for monthly precipitation data in the south west of Europe, but do not consider extreme values. Their method of homogenisation involves the removal of values above a given threshold (defined by interquartile range and the value of the third quartile) and their subsequent replacement with indicative dummy figures, to be 'later restored for specific studies concerning extreme values'. In other studies, extremes may be rejected and replaced by missing value codes (Gonzalez Rouco *et al.*, 2001; Mitchell and Jones, 2005). The corrections that are rendered by a replacement approach are of little use in studies such as this thesis unless looking at frequencies of occurrence alone. When studying extremes of climate, value adjustment is not a particularly valid option as outliers may be of particular relevance (Gonzalez-Rouco *et al.*, 2001). Issues also arise from the possibility that true extremes may be rejected, or that outliers may be erroneously considered as true extremes (Manton *et al.*, 2001). The majority of techniques for homogenisation have not been constructed for use with daily data or studies in extreme behaviour (Peterson, 1998), and correction methodologies that are in current use may not work well in either case (Guttman, 1998). Thus only detection techniques are used in this study, and stations suspected of heterogeneity are rejected outright without attempts at correction.

The majority of stations used here have been supplied by a body which has conducted its own homogeneity testing, KNMI. The KNMI methodology is described by Wijngaard *et al.* (2003), and a large proportion of the inconsistencies identified are explainable by metadata. KNMI have utilised not one, but four individual tests and assessed homogeneity of daily data based upon the collected results. Each of these methods are detailed further in Section 3.3.1. For the purposes of this study, any station classified by KNMI as 'suspect' (three or four out of the four tests reject homogeneity) or 'doubtful' (two tests reject homogeneity) was rejected, leaving only 'useful' data (one or no tests reject homogeneity). Thus this study follows the advice of Wijngaard *et al.* (2003), ensuring that data can be utilised for both variability and trend analysis.

Data not tested by KNMI were tested using their data as a reference series for spatial or temporal inconsistency using inter-correlation and analysis for detecting suspect spatially discontinuous trends (Manton *et al.*, 2001). Step detection tests such as that used by Vincent *et al.* (2002) have been effective with daily extreme data temperature (for Canada), but their method utilises monthly averages to isolate large-scale and systematic heterogeneity and may be adversely affected by highly variable topography (as seen in the Mediterranean basin) due to multi-station averages. As with Wjingaard (2003) relative testing was not used in its standard form (i.e. comparing many stations to one reference station) due to changes in topography and the sparse spatial density of the station network. Instead comparisons for one station were made with numerous nearby stations. From these tests a further four stations were rejected (Rhodos, Bedonia, Albacete, and Calzada). Having pared the data set down to remove incomplete stations (Haylock and Goodess, 2004; Klein-Tank and Können 2003), and those that are inhomogenous, the total number of stations available for analysis becomes 84 (Table 3.1).

As discussed above the data used for this study have undergone rigorous homogeneity testing. Together the 4 statistical tests utilized offer a comprehensive approach to detection, and are the standard normal heterogeneity test (Alexanderson, 1986), the Buishand range test (Buishand, 1982), the Pettitt test (Pettitt, 1979), and the Von Neumann ratio test (Von Neumann, 1941).

The Standard Normal Heterogeneity Test (SNHT) was introduced by Alexanderson (1986), and assumes that for a test station (Y) the test values (Y_i to Y_k) and a reference regional average series ($\bar{Y}$) are proportional to each other, as does the Buishand Range Test (see below). A test statistic (as used by Wijngaard *et al.*, 2003) can be formulated that assesses the likelihood of breaks in the mean between k years at the beginning of the record, and n - k years at the end.

$$T(k) = k\bar{z}_1^2 + (n-k)\bar{z}_2^2 \quad k = 1, ..., n \tag{3.1}$$

Where:

$$\bar{z}_1 = \frac{1}{k}\sum_{i=1}^{k}(Y_i - \bar{Y})/s \quad and \quad \bar{z}_2 = \frac{1}{n-k}\sum_{i=k+1}^{n}(Y_i - \bar{Y})/s \tag{3.2}$$

s is the standard deviation, and $T(k)$ maximises near the year $k = K$ if a break occurs at year k. The test statistic is then shown as:

$$T_0 = \max_{1 \le k \le n} T(k) \tag{3.3}$$

The Buishand Range Test (Buishand, 1982) gives a value S^*_k that is sensitive to 'systematic deviations' (Wijngaard *et al.*, 2003) of Y_i with respect to the regional mean, and that therefore fluctuates around zero if a series is homogenous, and deviates from zero if it is heterogenous:

$$S^*_0 = 0 \quad and \quad S^*_k = \sum_{i=1}^{k}(Y_i - \bar{Y}) \quad and \quad k = 1, ..., n \tag{3.4}$$

S^*_k maximises near the year $k = K$ if the series exhibits a negative break at year K, and minimises if a positive shift is present. R, the 'rescaled adjusted range', allows for a test of shift significance, and is given by:

$$R = (\max_{0 \le k < n} S^*_k - \min_{0 \le k < n} S^*_k)/s \tag{3.5}$$

Critical values for $R/\sqrt{n}$ are given in Buishand (1982) and Wijngaard *et al.* (2003)

If year K shows a break in the time series being studied, the Pettitt test (a non-parametric rank test) supplies a value that maximises or minimises near $k = K$, utilising the ranks $r_1, ... r_n$ of $Y_1, ... Y_n$ (Pettitt, 1979). Unlike the previous test, it does not require a reference series. Where X_E represents a break in year E:

$$X_E = \max_{1 \le k \le n} |X_K| \tag{3.6}$$

The significance level of X_E is given by Pettitt (1979), and X_K:

$$X = 2\sum_{i=1}^{k} r_i - k(n+1) \quad k = 1, ..., n \tag{3.7}$$

The Von Neumann ratio test statistic (which cannot give information regarding where in the series a shift occurs) provides a ratio between the mean square successive difference from year to year and the variance of a time series (Von Neumann, 1941):

$$N = \sum_{i=1}^{n-1}(Y_i - Y_{i+1})^2 / \sum_{i=1}^{n}(Y_i - \bar{Y})^2 \qquad \textbf{(3.8)}$$

Homogenous time series give values of N close to *2*, N may be lower if there is a break in the mean or higher if variations in the mean fluctuate rapidly.

3.3.2 Interpolation

When constructing indices from gridded data, as required here for circulation indices (Section 3.5.2), there is sometimes need for a method that can generate representative data at a specified point. Sixteen point Bessel interpolation (Chakravarti *et al.*,1967; Kotz and Johnson, 1982; Palutikof *et al.*, 1997) can be used to obtain information about a point from a grid of data by means of multi-directional geometrically weighted averaging (Chakravarti *et al.*,1967; Kotz and Johnson, 1982). For a given function $f(\cdot)$, tabulated h points apart, there is a value $f(t)$ within the interval t_0 to t_0+h. If $f(t)=y_{(t-t0)/h}$, $(t-t_0)/h=x$, and $v=x-1/2$, then:

$$y_x = P_{2n+1}(x)$$

$$= \frac{y_0 + y_1}{2} + v\Delta y_0 + \frac{v^2 - \frac{1}{4}\Delta^2 y_{-1} + \Delta^2 y_0}{2} + \frac{v(v^2 - \frac{1}{4})}{3!}\Delta^3 y_{-1}$$

$$+ \frac{(v^2 - \frac{1}{4})(v^2 - \frac{9}{4})}{4!} \times \frac{\Delta^4 y_{-2} + \Delta^2 y_{-1}}{2} + ... \qquad \textbf{(3.9)}$$

$$+[(2n+1)!]^{-1}v(v^2 - \frac{1}{4})(v^2 - \frac{9}{4})...$$

$$\times[v^2 - (2n-1)^2/4]\Delta^{2n+1}y_{-n'}$$

Where Δ^r is the *rth*-order forward difference. For interpolating a value at the midpoint between successive tabulate values where $|v| < \dfrac{1}{4}$.

3.3.3 The Kendall's Tau method

Changes in Mediterranean climate are important to this study. To appropriately estimate changes over time in representative indices of Mediterranean extreme climate (Section 3.4.1), a method of assessing trend behaviour is required. Kendall's Tau (Sen, 1968; Kotz and Johnson, 1983; Kunkel *et al.*, 1999a; Lins and Slack, 1999) is a test for both linear and non-linear trends that makes no strong assumption (i.e. it is non-parametric) about the data concerned. These are useful properties when dealing with potentially non-linear extremes of climate. Kendall's Tau relies on the connection of all data pairs (e.g. y1 and y2, y2 and y3, y1 and y3…) and a ratio between the number of resulting slopes which possess upward or downward gradient. If the majority have a downward (upward) gradient, the data is considered to possess a negative (positive) trend. If Kendall's Tau reaches zero, there is no trend evident in the data. Values nearing 1 and –1 imply a vertical distribution (x is constant, y varies) to the data. Kendall's Tau (τ) is given by the following equation:

$$\tau = \frac{number\,of\,positive\,slopes - number\,of\,negative\,slopes}{total\,number\,of\,segments} \qquad (3.10)$$

A Z-test can then be conducted using an approximation to the normal distribution and Tau as a test-statistic. Assuming a normal distribution of Tau causes the mean of Tau to become zero, and the standard deviation of Tau to become:

$$SDof\tau = \sqrt{\frac{2(2n+5)}{9n(n-1)}} \qquad (3.11)$$

Z is then:

$$z = \frac{\tau - \bar{\tau}}{SDof\tau}$$ (3.12)

3.3.4 Spearman rank correlation

Correlation is a method of determining the magnitude of shared variance between variables. This method cannot (statistically) prove a causal mechanism, but can imply a causal link (Wilks, 1995; Von Storch and Zwiers, 1999), again part of an important theme for this study. To that end all indices are tested for correlation with all other indices. The sample correlation of a set of bivariate observations is generally calculated as the ratio (r_{xy}) between the covariance of the given x and y sample ($cov(x,y)$), and the product of the standard deviations of x and y ($s_x s_y$), as given by equation 3.13 (Wilks, 1995):

$$r_{xy} = \frac{cov(x, y)}{s_x s_y}$$ (3.13)

In order to allow for efficient calculation of *r*, this equation can be broken down into two components, where the numerator can be expanded to equation 3.14, and each part of the denominator as shown in 3.15:

$$cov(x, y) = \sum_{i=1}^{n}(x_i y_i) - \frac{1}{n}[\sum_{i=1}^{n}(x_i)][\sum_{i=1}^{n}(y_i)]$$ (3.14)

$$s_x = [\frac{\sum(x_i^2) - n\bar{x}^2}{n - 1}]^{1/2}$$ (3.15)

Where 3.15 can also be applied for s_y.

The equation given above (3.13) provides a value bounded between 1 and –1 that represents the linear association between x and y, with values of 1 and –1 implying 'perfect' positive or negative covariance. Further, the square of r (r^2) gives the proportion of variance that is linearly explained in one variable by the other.

However, this method (the Pearson product-moment correlation) has some distinct limitations. The first is that it is sensitive to outliers, and one or two extreme values can greatly increase or decrease the apparent correlation. The second issue inherent in the use of the Pearson correlation method is that it is not robust for non-linear relationships. One way of avoiding both of these issues is through the use of the Spearman Rank Correlation (Wilks, 1995), similar to the method given above, except that it is performed upon the ranks of the data rather than the values. A given series (e.g. 1.43, 4.24, 3.56, 5.84, 5.81, 2.45, 6.23) is substituted for the sequential rank of magnitude for each value (e.g.1, 4, 3, 6, 5, 2, 7). This allows equation 3.13 to be greatly simplified, yet still provide the same result:

$$r_{rank} = 1 - \frac{6 \sum_{i=1}^{n} D_i^2}{n(n^2 - 1)} \qquad \textbf{(3.16)}$$

Where *D* represents the difference in ranks between each (i) pair of data values. This formulation of *r* represents not the strength of linear relationships, but of *monotonic* (consistently increasing or decreasing) relationships, and it is the formulation for correlation coefficients used in this study. In addition, in all cases where correlations are quoted they have been calculated with autocorrelation taken into account to ensure that correlations are not due to mutual trend behaviour alone.

3.3.5 Significance and stability testing

To determine whether trends or correlations discovered by the two previous methods are likely to reflect real behaviour, all trends and correlations considered in this study are tested for 'significance'. Significance testing relies on the use of a null

distribution, the distribution of samples given that the null hypothesis is true, where in this case the null hypothesis is that a particular trend or correlation has occurred purely by random chance. Here the test statistics are Z (Equation 3.12) and r (Equation 3.16) and null distributions are approximated by the normal (Kotz and Johnson, 1983) and Student's-t distributions respectively (Wilks, 1995). Results must then be sufficiently improbable within the null distribution (i.e. sufficiently close to the tail) to be considered significant. In this study a trend is considered significant if it satisfies testing at the 0.05 level or below (i.e. it has only a 5% probability of occurring by chance) (Kotz and Johnson, 1983) and correlation (r) values are qualified as representing moderate (significant at the 0.10 level), good/highly significant (the 0.01 level), or very good/very highly significant (the 0.001 level) correlations, with the probability of occurring by random chance decreasing by an order of magnitude between each level (Table 3.2).

Correlation and trend values have also been tested for stability. Any correlation included in this study is not only significant for the whole of the test period, but also for sub periods from 1960-1980, and 1980-2000.

3.3.6 Principal component analysis (PCA)

Principal component analysis is a methodology in wide usage by the climatological community that allows for the spatial and temporal analysis of the variability of physical fields (Preisendorfer, 1988; Esteban-Parra *et al*., 1998; Rodriguez-Puebla *et al*., 1998; Maheras *et al*., 1999a; Serrano *et al*., 1999; Quadrelli *et al*., 2001; Bordi and Sutera, 2001). Researchers have utilised PCA (also termed Empirical Orthogonal Analysis, or EOF) to investigate centres of variance in a number of data (Maheras *et al*., 1999a; Serrano *et al*., 1999; Quadrelli *et al*., 2001; Bordi and Sutera, 2002), but its main function is to reduce dimensionality of a data set (Preisendorfer, 1988; Jolliffe, 1990). In this study, the NCEP data (Section 3.2.2) for SLP, Z500 and SHM fields (Section 2.3.1) are subjected to PCA and both applications are useful. The PCA method can be used to study the climatology of the Mediterranean region (through centres of variance) in terms of circulation regimes (Section 2.3.3 and

3.5.5), and in an attempt to include otherwise unwieldy multi-dimensional data (Sections 2.3.1 and 3.2.2) as model predictors representing those regimes (Section 3.5.4). Wilks (1995), Jolliffe (1990), and Priesendorfer (1988), offer good descriptions of PCA, and the method is summarised from those works below.

If a data set contains points that are substantially inter-correlated then it also contains redundant information. PCA seeks to remove this redundancy by drawing functions from a data set that together describe the majority of variance information without repetition. The factors of these functions are the 'principal components' of the data, and a large number of functions can generally be sacrificed at the expense of very little in the way of explained variance. This leaves the researcher with a greatly reduced data set that still account for the majority of variance. Atmospheric fields tend to display a large amount of redundancy as concurrent points are often interdependent and they are therefore well suited to this form of treatment.

Principal components are given by eigenvectors of the data-sets variance-covariance matrix multiplied by the data set anomalies (i.e., the data set with the mean subtracted from the original). The variance-covariance matrix is the anomaly data (Eqn. 3.18), multiplied by its own transpose and divided by *n*-1 (Eqn 3.19), where *n* is the number of observations, or row-length in the case of 2-D matrices.

$$x' = x - \bar{x} = \begin{bmatrix} x_1 \\ x_2 \\ x_3 \\ . \\ . \\ . \\ x_n \end{bmatrix} - \begin{bmatrix} \bar{x}_1 \\ \bar{x}_2 \\ \bar{x}_3 \\ . \\ . \\ . \\ \bar{x}_n \end{bmatrix} \tag{3.18}$$

$$[S] = \frac{x'x^T}{n-1} \tag{3.19}$$

The result is a square matrix *[S]* whose diagonal represents the sample variances of the anomaly data set's rows (or a particular set of observations for greater

dimensionality), and whose other elements express inter-row covariance. Eigenvectors *(e)* are those vectors that can be multiplied by either the originating matrix or a scalar value (an eigenvalue λ) to give the same result (Eqn. 3.20).

$$[S]e = \lambda e \qquad (3.20)$$

In most cases there will be as many eigenvectors as there are rows and columns in the original matrix, and in the case of symmetric matrices (such as the covariance-variance matrix) each eigenvector of the matrix is orthogonal to every other eigenvector. This is the property that ensures successive principal components explain exclusive proportions of variance. The equation for each (*m*th) principal component (u_m) is then:

$$u_m = e_m^T x' = \sum_{n=1}^{N} e_{nm} x_n', \quad n = 1, ..., N \qquad (3.21)$$

After a geophysical field that varies with time (a 3 dimensional matrix) is subjected to PCA, two useful products are available. The first of these are a number of principal component score time series (PCs) equal in quantity to the number of matrix elements in the field (without time) that are orthogonal to each other. The second useful product is a set of weightings (or 'loadings') for each PC that numerically describe the way a given mode of variance affects each field element, and can then be plotted in map format to display centres of variance. These loadings are simply the elements of each eigenvector resulting from the variance-covariance matrix detailed above.

The loading plots can be interpreted directly as modes of variance in the field, but care must be taken to remember that each mode is orthogonal to every other mode (as they are eigenvectors). Discrete and large loading anomalies can be taken to represent areas where the relevant PC is strong, and thus where orthogonal modes of variance are the most apparent in the field's behaviour. Where these structures resemble known phenomenon (such as the centres of action described in Section 2.2.2) variance

can sometimes be attributed to those processes. If a persistent loading anomaly for a pressure PC is apparent over the Azores for example, then that indicates high levels of relative variability in that region. If the shape of the anomaly is consistent with the southward centre of the North Atlantic Oscillation then the PC under consideration can be assumed to represent some measure of the NAO phenomenon. If a loading anomaly pattern displays no apparent relationship to known phenomenon, and displays unlikely characteristics (such as opposing poles of variance in each of the corners of the region), it may be rejected as an artefact of orthogonality (Priesendorfer 1988; Wilks, 1995). Such artefacts are generally more common for low variance components than high variance components (Wilks, 1995).

The fall-off of variance explained with each successive PC tends to be roughly exponential, and PCs can also be rejected when they fall below a certain proportion of variance or lie below a level given by the 'Scree test'. The Scree test simply plots the amount of variance explained for each component in succession and gives the level where the curve starts to flatten as a cut-off point. In this study components are rejected if they fall below the Scree test cut-off point or if the amount of variance explained is less than 0.04 (Briffa *et al.*, 1983) (see Table 3.3 for a summary of retained components). The use of both methods ensures a high total explained variance (the variance explained by all retained components taken together), while ensuring that the number of retained components is low (Fig. 3.1). It is the process of rejecting components that reduces the dimensionality of a given atmospheric field, and allows the large amounts of data associated with atmospheric fields (that vary with time) to be included as model predictors (Section 3.5.4) in this study.
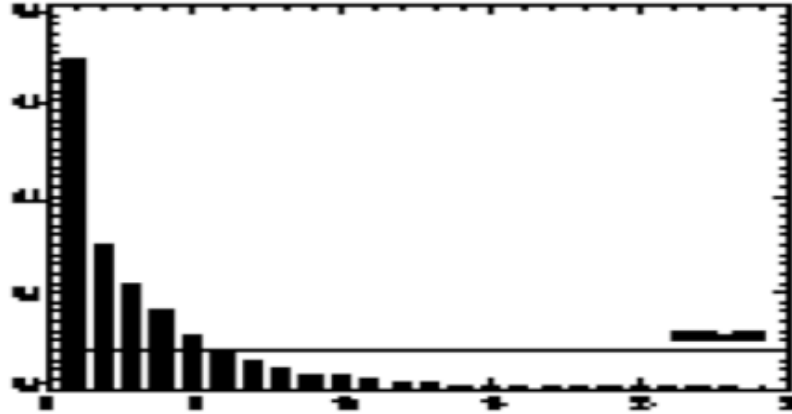
Figure 3.1: Fall off in variance for principal components. Values are average variance for first 25 PCA components (ordered by amount of variance explained) of seasonal fields (SLP, Z500, and SHM).

3.4 Climate predictand variables

3.4.1 Defining extremes

The indices of extremes used in this study (Chapter 1.3) take the form of the STARDEX top ten, a subset of the indices recommended by the Research Programme on Climate Variability and Predictability (CLIVAR) (Peterson *et al*., 2001) and the joint working group on climate change detection of the World Meteorological Organization's Commission for Climatology (WMO-CCL). The selected indices encompass complimentary measures of threshold excedance (frequency), duration (persistence) and magnitude that are not highly correlated, are robust, and are comparable across regions (Frich *et al*., 2002), with a minimum of physical overlap, and a likely relevance for impacts purposes (Goodess *et al*., 2006). For this study, each of the ten indices of extremes were calculated seasonally from daily station data using the STARDEX 'Indices of Extremes' program (available at http://www.cru.uea.ac.uk/cru/projects /stardex/), with equations that can be found in Haylock (2004), detailed below. A summary of the predictands used in this study can be found in Table 3.4

For complex conditions such as drought, simple indices defined only from precipitation have been found to be as useful (McKee *et al.*, 1995, 1993; Guttman, 1997; Lloyd-Hughes and Saunders, 2002) as more complex indices that may possess hidden weaknesses (Alley, 1984; Heddinghaus and Sabol, 1991; Guttman *et al.*, 1992). In addition, a growing number of studies (Jones *et al.*, 1999a; IPCC, 2001; Frich *et al.*, 2002; Klein-Tank and Können, 2003; Haylock and Goodess, 2004) are conducting work with indices similar to those used here, making for a body of easily comparable research (Klein-Tank *et al.*, 2003). However, care should be taken when referring to indices across studies as similar terms may have different definitions. For instance, TX90 and TN10 (shown below), both measured in °C, differ from the TX90p and TN10p indices used by Klein Tank and Können (2003).

Warm Days (TX90)

This index is a measure of the temperature at which a day becomes unusually warm relative to the period of study. 'Warm days' are those whose temperature exceeds a threshold defined by the 90th percentile of the daily maximum temperature (Tmax) distribution. Above the 90th percentile of a distribution, events are generally of a low enough frequency and a high enough magnitude that society may find conditions difficult to respond to, generally requiring coping strategy in place (Jessamy, 2003) to avoid adverse affects such as those experienced during the summer of 2003 (Beniston, 2004). TX90 is the calendar day 90th percentile of daily (*i*) maximum temperatures (*Tx*) for a season (*j*),

$$TX90 = Tx_{ij}90 \qquad \text{(3.22)}$$

Heatwave Duration (HWDI)

This index measures the duration of temperature behaviour consistent with the term 'heatwave', i.e. persistently anomalous high temperatures. These events are rare, but often highly debilitating. During summer and in combination with a high Warm Days index, high values of this index may directly represent heatwave behaviour consistent with the European summer of 2003 (Beniston, 2004). The duration of (Alpine) winter warm spell conditions, when departures from mean temperature may exceed those for summer (15°C from the mean) can also be represented by this index

(Beniston, 2005). Winter warm spells, although not generally perceived as extreme events, can create a large number of significant impacts (Beniston, 2005). HWDI is the largest number of consecutive days in a given season (j) for which daily (i) maximum temperature (Tx):

$$Tx_{ij} > TX90_{inorm} + 5 \tag{3.23}$$

Where *TX90* is the calendar day 90th percentile of temperature calculated for a 5 day window centred on each day of the period in turn.

Cold Nights (TN10)

This index is the inverse of TX90. TN10 is the 10th percentile of the daily minimum temperature (Tmin) distribution and it typifies the temperature at which a night becomes unusually cold. Much in the same way that unusually Warm Days may debilitate people, cattle, and crops (in events such as the 2003 heatwave, see Chapter 2.4.2), particularly Cold Nights may be the cause of elderly and infant mortality and arable failure (cf. the Balkan cold snap event of 1987, Chapter 2.4.2). TN10 is the 10th percentile of daily (i) minimum temperatures (Tn) for a season (j).

$$TN10 = Tn_{ij}10 \tag{3.24}$$

Frost Days (TNFD)

Water freezes at or near to 0˚C, and when it does, frost occurs. The frost days index measures air frosts (Frich *et al.*, 2002) and is one of only two used in this study with an absolute threshold, representing the number of days in a season during which frost may form. If daily minimum temperature drops below 0˚C, that day is a Frost Day. The reason for such a well-defined statistical threshold is purely physical, as frost may damage crops, particularly in the Mediterranean (Xoplaki *et al.*, 2001). TNFD is the number of days in a season (j) for which daily (i) minimum temperature (Tn).

$$Tn_{ij} < 0°C \tag{3.25}$$

Very Wet Days (PQ90)

The Very Wet Days index is the 90th percentile of daily total rainfall calculated seasonally: it is the precipitation analogue of the Warm Days index and represents heavy rainfall. Changes to measures of heavy rainfall may also represent changes in the frequency of flood events (Suppiah and Hennesy, 1998). PQ90 is the 90th percentile of daily (*i*) rainfall (*R*) for a season (*j*).

$$PQ90 = R_{ij}90 \qquad\qquad (3.26)$$

Five-Day Maximum Rainfall (PX5D)

Although large volumes of rain can cause floods on a single day basis (flash floods), more common are those that are the result of persistent rainfall over a short period (e.g. 3-5 days, see Chapter 2.4.2). High values of this index, (and that for Rainfall Intensity, or Wet Days) may be linked to flooding in larger catchments (Goodess *et al.* 2006). R_{kj} is the precipitation amount for a period (*k*) of *N* days in a season (*j*) for which daily (*i*) precipitation exceeds wd_{cutoff}, set to 1mm, and *N=5*:

$$PX5D = \max(R_{kj}) \qquad\qquad (3.27)$$

Consecutive Dry Days (PCDD)

This is the second index that utilises an absolute threshold, and it does so because the rainfall distribution is fixed at its lower bound (i.e. 0mm). Frich *et al.* (2002) state that PCDD can potentially become a useful drought indicator, but when using it as such care should be taken to set an appropriate 'dry day' threshold. In this study a relatively low threshold of 1 mm is used (rather than the 10mm threshold used by Frich *et al.*, 2002). In the Mediterranean persistent periods that display less than 5 or 10mm a day are not as uncommon as for the rest of Europe (Martín-Vide and Gomez, 1999). *PCDD* is the largest number of consecutive days in a season (*j*) for which daily (*i*) precipitation does not exceed wd_{cutoff}, set to 1mm:

$$R_{ij} \leq wd_{cutoff} \qquad\qquad (3.28)$$

Rainfall Intensity (PINT)

Due to the zero lower bound, averages of rainfall may not be as useful as other measures. Rainfall Intensity represents the amount of rain per rainy day, avoiding the lower bound problem. A combination of this index, the Consecutive Dry Days index and PF90 (below) may show whether or not Mediterranean rainfall is becoming less frequent but more intense, as suggested by Chapter 2.4.4 (a tendency that would exacerbate both flooding and drought), or otherwise. The mean precipitation ($PINT_j$) on rain days ($w(R>wd_{cutoff})$) with wd_{cutoff} set to 1mm, for a period (j) with daily precipitation (R_{wj}) can be shown as:

$$PINT_j = \sum_{w=1}^{W} R_{wj}/W \tag{3.29}$$

Number Of Days Classed As Very Wet (PN90)

The Number Of Days Classed As Very Wet index is self-descriptive. It is the percentage of days in a given period that have more rainfall than the value given by the Very Wet Days index. In combination with PF90 it allows for a measure of the intensity of extreme events by comparing the relative amount and relative frequency of rain from such events. For a given period (j) PN90 is the number of wet days where the amount of rainfall (R_{wj}) is greater than the long term 90th percentile.

$$R_{wj} > R_{wn}90 \tag{3.30}$$

Fraction Of Rainfall Due To Very Wet Days (PF90)

This index represents the amount of extreme rain, per amount of rain, from very rainy days, another way of typifying a precipitation distribution without being hampered by the zero lower bound. On rain days ($w(R>wd_{cutoff})$) with wd_{cutoff} set to 1mm, for a period (j) with daily precipitation (R_{wj}) and the 90th percentile of the wet day precipitation for that period ($R_{wn}90$), the fraction of rainfall from events that yield more rainfall than the long-term 90th percentile *PF90* is:

$$PF90 = \sum_{w=1}^{W} R_{wj} / R_j \, , \, where \, \, R_{wj} > R_{wn}90 \qquad \textbf{(3.31)}$$

In addition to the above indices, all of the analyses shown later in this chapter (Section 3.4) were conducted with seasonally averaged daily mean temperature (TAVG), maximum temperature (TMAX), minimum temperature (TMIN) and mean precipitation (PREC).

3.4.2 Seasonal and spatial variation of climate indices

Having detailed the indices of extreme behaviour that are used in this study, and how they are statistically related to each other, further analysis benefits from a description of the variation of these indices from season to season and across the Mediterranean basin. Geographical factors may have a consistent effect upon both temperature and precipitation, but values of the indices described in the previous section change with the season and varying circulation. Figures 3.2-3.9 show values for the indices of extreme climate averaged over the period 1958-2000 divided by season, temperature, and precipitation. All figures given below are averages over the 1958-2000 period.

Winter

Winter Mediterranean temperatures average 6.5°C, but as described in Chapter 2 an important global control on temperature is latitude (Fig. 3.2). In general temperatures increase and the occurrence of frost decreases with decreasing latitude. Winter low temperatures occur along the northern edge of the basin (Clermont Ferrand and Lyon in France, Paganella in Italy, Zagreb in Croatia, Calarasi in Romania), and highs toward the southern edge (Dar El Beida in Algeria, Ierapetra in Greece). The latitude effect, in part, creates an average winter temperature (TAVG) range (between stations of similar altitude, Dar El Beida and Lazzaro in Italy) of around 10°C (between 12°C and 2°C, respectively). The difference between southern TX90 values and

northern TN10 values (again between Dar El Beida and Lazzaro) is much greater, at 28°C (21°C and -7°C).

Throughout the central highland region of Iberia, the northern and southern peaks of Italy (the Alps, Prizzi, Monte Scuro, and Trevico), and the highest regions of Greece (Tripoli, Ioannina and Kozani), temperatures are consistently lower than neighbouring lowland regions (Fig 3.2). All temperature indices display values decreasing with height (Chapter 2.2.2), an effect much more noticeable for indices of warmth (TMAX and TX90) than cold (TMIN and TN10). The number of frost days increases with height, however, as suggested by Beniston (2005) for the Alps, winter warm spell (i.e. heatwave) persistence across parts of Spain, Italy (including the Alps) and Greece also increases with height. Between Prat de Llobregat (6m altitude) and Montseny Turo (1706m altitude) in eastern Spain (65km apart) for example, average winter TAVG, TMAX, TN10 and TX90 values decrease by around 8°C (TN10 decreases from 1.6°C to -6.2°C), an additional 58 days experience frost (from 4 days to 62), and heatwaves lengthen by 0.8 of a day (from 2.8 days to 3.6). The lowest Mediterranean winter temperatures in terms of both high and low extremes (TMIN, TN10, TMAX, TX90), and the number of days with frost, all occur over 900m in altitude, for:

- o Montseny Turo (Spain),
- o Penhas Douradas (Portugal),
- o Paganella, Ligonchio, and Monte Scuro (Italy),
- o Ioannina, and Kozani (Greece).

Peaks with similar altitudes (Montseny Turo and Monte Scuro, around 1700m), show marginally lower temperatures (-0.2°C) and a greater incidence of frost (+1 day) with greater latitude. Paganella (at both 2125m in height and toward the northern edge of Italy) consistently displays the lowest of Mediterranean winter temperatures (TN10 of -11°C, TX90 of 4°C, TNFD of 82 days).

Winter warm spell behaviour at height is less dependent on latitude, and more sensitive to altitude. However, closer to sea level, winter warm spells are relatively long

(over 4 days) across the west of Iberia and to the east of the Balkan mountains, and low (less than 3 days) throughout the majority of the central and the remainder of the eastern basins. This winter pattern reflects regions particularly susceptible to persistent westerly and south westerly warming flow from the Atlantic (Barry and Chorley, 1998; Maheras *et al.*, 1999a), a sheltered area (to the east of the Balkan mountain chain) associated with winter pressure systems that may remain stationary for up to two weeks (Kallos *et al.*, 1993), and southerly or south westerly flow from Africa (Maheras *et al.*, 1999a).

Other winter effects not directly dependent upon either latitude or altitude alter temperatures indices (TAVG, TMIN, TMAX, TN10, TX90, TNFD) in Valencia and the north west of the Balkans. In Valencia, low temperature extremes (TMIN and TN10) are not as low (by 2.5°C) as those for nearby stations (TN10 of 8.7°C for Valencia, 6.2°C for Alcantarilla). Due to pressure systems located to the north east of Valencia the region may experience periods of easterly flow (Sumner *et al.*, 1993). During winter such flow is likely to provide warmer air than winds sourced from within the peninsula due to the relative heating effect of the Mediterranean Sea (Chapter 2.2.2), which also ensures that in general coastal stations are warmer than those in land. Frost days in particular are much less common (values less than 5 days) for coastal stations. In the latter (eastern basin) case winter circulation occasionally draws air down from the north along the western coast of the Balkans and toward Thessaloniki (forming the Bora and Varadarac winds, Table 2.3). The area associated with these winds shows lower winter temperature indices (by about 3°C) and a substantially greater incidence of frost spells (by 30 days) than neighbouring regions or those at similar latitudes and altitudes.

Although rainfall generally displays a positive correlation with latitude, such a relationship is not evident for the Mediterranean winter (Chapter 2.2.1), neither is there a consistent response to altitude. Instead, indices of extreme precipitation (Fig 3.3) vary from region to region in a manner more consistent with flow direction and the paths of cyclones (Table 2.2).

The largest volumes of winter rainfall occur upon the northwest Atlantic coast of Spain (i.e. La Coruna) and across northern Portugal. These regions are the parts of the target area most susceptible to cyclones entering the basin from the Atlantic (Barry and

Chorley, 1998). Average PREC values are high (around 8mm), as are PQ90 values (around 37mm), and measures of both rainfall intensity (PINT) and the prevalence of heavy rain events (PN90) show much higher values in the north west Iberian region than for the majority of the basin (around 17mm/day, and 3.9 days, respectively). As might be expected from these values, persistent rain events provide very large volumes of precipitation (167mm), and periods without rainfall are short (14 days). Because rainfall is generally heavy in the north west Iberian region (Martín-Vide, 2004) the percentage of rainfall provided by very heavy (rare) events is not particularly high (27%). South western France and northern Spain show similar behaviour, although rainfall is generally not as heavy (PREC of 4mm), a greater proportion of rainfall comes from heavy events (30%).

During winter, the driest area in the Mediterranean basin is the Murcia region of south east Spain (Martín-Vide and Gomez, 1999), where periods without rainfall are among the longest in the basin (PCDD of 33 days). Atlantic influences are less significant for this region than the rest of Spain (Romero *et al.,* 1998a), and rainfall amounts are more dependent upon easterly/south easterly flow (Goodess, 2000), For Murcia average winter rainfall is low (0.75mm), and the number of heavy rain events is low (1 day), but as rainfall is so rare the proportion of rain to come from such events is relatively high (35%) (Martín-Vide, 2004).

To the north east, north, and north west of the Gulf of Genoa rainfall is particularly intense (between 13mm/day, Nice and 19mm/day, Bosco). Average rainfall is not high (around 4mm), dry periods can be long (around 17 days) and there are not very many heavy rainfall events (2 days), but the proportion of rain to come from those events is high (34%), and extreme rain events can produce the largest volumes of precipitation to occur from single (PQ90 of 44.7mm at Bosco) or prolonged (PX5D of 180mm at the same site) events within the basin. The Gulf of Genoa is one of the principal areas of Mediterranean cyclogenesis, and the figures above may reflect the amount of moisture locally advected from the Mediterranean sea (Trigo. 1999).

Areas also experiencing large volumes of winter rainfall include the west coasts of Sardinia, southern Italy, Greece and Turkey. These regions are subject to cyclones that have travelled across the Mediterranean (including those that have been regenerated

from Genoan cyclones, Table 2.2) and where such depressions track across western coasts high levels of precipitation may occur (Chapter 2.2). The eastern basin (Greece, and Greek stations near the coast of Turkey) is generally not as wet (PREC of around 4.2mm) as the north west Iberian peninsula, and periods without rain are not as short (19 days). However, values for PQ90 (27.5mm), PF90 (31%), PN90 (3 days), and PX5D (101mm) generally exceed those for the south of France and northern Spain. Rainfall intensity is also high, and can (in places) equal or exceed values for the Gulf of Genoa (around 14mm/day). With the exception of the anomalously high rainfall that occurs to the north west of the Iberian peninsula, eastern basin winter rainfall is generally higher than that for the west. For the southern parts of the central basin (Sardinia and southern Italy), and in terms of the ratio between heavy and light events (i.e. PN90 and PF90) the western coasts of the region display similar behaviour to that evident for the western coasts of the eastern basin.

Spring

During the spring, Mediterranean average temperatures (Fig 3.4) increase by 5.7°C (to 12.2°C). However, although features similar to those for winter can be observed in the spring spatial distribution of extreme temperature indices, the differences between north and south, and between stations at high and low altitude are smaller for all but the highest stations (Paganella, Monte Scuro, Penhas Dourados, and Montseny Turo). Between Dar El Beida in Algeria and Lazzaro in Italy there is an average temperature difference of 3°C (between 15°C and 12°C TAVG, respectively), and there is only a 0.5°C difference between northern and southern TX90 values (10°C difference in winter). The range in extreme temperatures between these stations (between southern TX90 and northern TN10) also decreases (from a winter range of 28°C) to 26°C (26°C TX90 and 0°C TN10).

Between northern, high altitude TN10 values (-7.7°C for Paganella) and southern low altitude TX90 values (26°C for Dar El Beida) there is, however, an increase in range (from 29°C in winter to over 35°C in spring). In spring there are greater differences in temperature and heatwave duration between very high stations and their low-lying neighbours than for winter. Between Montseny Turo and Prat de Llobregat the differences between TAVG, TMAX, TMIN, TN10 and TX90 increase to

10°C. Spring heatwaves last a day longer at high altitude than at stations near sea level. This tendency is due to a greater seasonal warming and lengthening (from winter to spring) of low-lying temperatures and HWDI values than for those at height, which remain low in the former case and high in the latter. For stations of slightly lower altitude (such as Soria, central Spain, 1082m) this relationship no longer holds, and the shift toward a more homogenous spring distribution is more apparent, particularly for extreme high temperatures (0.3°C TX90 difference between Soria and Valencia, stations of similar latitude and differing altitude). In spring the number of days with frost decreases at both height and nearer sea level, such that frost occurrence below 350m is rare and high values of TNFD (up to 60 days) occur only at very high (above 1700m) stations and along the northern boundary of the target region.

During spring a contrast develops between east and west coast HWDI values for Iberia and the Balkans. From winter to spring, west coast heatwave periods lengthen, and east coast values decrease. Although the longest periods are at height, as detailed above (Paganella, 5.5 days), western Iberian and Balkan heatwaves are typically 1-1.5 days longer than their east coast counterparts (e.g. 4 days for Alvega, Portugal, 2.5 days for Valencia, eastern Spain). As detailed in Chapter 2.4.2 short Mediterranean heatwaves may result from a high pressure ridge drawing air from the south on their western flank, and down from the north on their eastern side (Colacino and Conte, 1995), heating and cooling respectively. A possible response to south-westerly flow is also evident in the distribution of spring TX90 values, which are higher by around 2°C in the south west of Iberia, Italy and the Balkan peninsula than in the south east.

In spring a latitudinal relationship within the distribution of extreme rainfall indices (Fig. 3.5) becomes apparent (Chapter 2.2.1). Quantities of rainfall and heavy rainfall are generally higher in the north (for PREC, PF90, PN90, and PX5D) and lower in the south (by around 1.5mm for PREC between southern Greece and northern Italy). This pattern is reversed for the dry days index (PCDD) (Lana et al., 2006). Although there are some areas that show an increase in rainfall, and some a decrease in rainfall relative to winter quantities, the range of values across the basin decreases slightly for all rainfall indices (by 2.7mm for PREC, 16mm for PQ90).

The wettest region within the basin remains the north west of the Iberian peninsula, with northern Spanish and southern French stations only slightly less wet, influenced by spring thunderstorms (Barry and Chorley, 1998). Similarly the Murcian region of Spain remains the driest region. In the latter case, average volumes of rainfall (PREC) increase by only marginal amounts (less than 0.1mm, to around 0.76mm). By comparison Coruna and northern Portugal show a significant decline in average rainfall (-2.5mm) from winter levels (around 8mm). For Coruna and Murcia the relationships between indices remain fairly unchanged from winter for all indices except PF90. The proportion of rainfall to come from heavy events increases in Coruna (+4% to 33%) and declines in Murcia (-3% to 30%). In the north west of Iberia the volume of rain produced from heavy rain events declines less (from winter to spring) than the volume of rain produced by 'normal' events, in the south east there is instead a spring shift in balance toward normal events.

Alpine Italy shows little in the way of a seasonal change in behaviour. There is a decrease in the number of consecutive dry days (by around 5 days), and volumes of rainfall and heavy rainfall increase slightly (PREC +0.3mm, PQ90 +1mm), but these changes are not as great as for other nearby stations which generally display declining rainfall (PREC -2.5mm) from winter to spring. This lack of significant change means that Alpine spring precipitation values are relatively very high, despite a slight decrease in intensity (-1mm/day PINT).

By comparison the stations of Zamora and Salamanca in central Spain show a substantial decrease from winter levels in all indices of extreme rainfall. Although these stations are not quite as dry (PREC of 1.25mm) as those in Murcia they are less susceptible to precipitation extremes. The Zamora/Salamanca region possesses the lowest spring PQ90 (9.5mm) and PINT (4.9mm/day) spring values for the Mediterranean, and PF90 (30%) and PX5D (31.5mm) values lower than those for Murcia, which remains the driest region largely due to lower average rainfall (0.85mm), longer dry periods (18 days PCDD for Zamora, 28 days for Murcia) and a lower frequency of extreme events (PN90 of 2 days for Zamora, 1 for Murcia).

In spring, Iberian and Greek stations develop a north west / south east (wet / dry) precipitation contrast evident in plots of PREC, PCDD, and PN90. For the remaining

indices the west coast / east coast contrast evident in winter persists. This seasonal decline in frequency of east coast rainfall is likely to be due to southern or eastern influence in the Balkans as spring rainfall in the eastern Aegean has been linked to cyclones centred to the south and south west of the region (Maheras *et al.*, 2004).

Summer

In summer (average temperature of 21°C) the temperature contrast between the northern and southern parts of the basin is reduced further, and differences are more evident between the cool north west and the warm south east (Fig. 3.6). TAVG, TMIN and TMAX values differ by around 1.5°C between Dar El Beida (TAVG 23.8°C) and Lazzaro (TAVG 22.2°C), but by 7°C between Santiago (in the north west of Spain) and the majority of south and south eastern stations (TAVG around 24°C for Dar El Beida, San Javier in Spain, Alghero in Sardinia, and Naxos in Greece). For more extreme temperatures (TX90) the contrast is less evident, values in the north west are similar to those in the south east (Santiago, 29°C, and San Javier, 30.5°C, TX90 values).

Very high altitude stations do not behave as described above, and as for other seasons possess consistently lower temperatures than nearby stations. However, from spring into summer high altitude TN10 values increase by more than low lying TX90 values, a reversal of the situation from winter into spring. The range in temperatures between Paganella and Dar El Beida is reduced from 35°C in spring to 32°C in summer. Between Montseny Turo and Prat de Llobregat the difference in TAVG, TMAX, TMIN, TX90, and TN10 temperatures are similar to those for winter (8°C), but values for heatwave duration are the same for both high and low stations (3.2 days). Frost days are rare during the Mediterranean summer, and only ever occur at height.

Although temperatures are higher during summer than for any other season, heatwave durations are not as consistent. Across Iberia summer HWDI values (average of 3.6 days) are shorter than those for spring by (on average) 1/2 a day. Values for the south of France (on average 3.5 days) and Italy (3.3 days) increase by the same figure. The lengths of Greek heatwaves (3.2 days) increase by only a marginal amount (0.1 of a day). However, the east coast (short heatwave) / west coast (long heatwave) HWDI contrast that appeared during spring persists in summer for Iberia (1.3 difference

between Alvega and Valencia), and strengthens for Italy (0.9 difference between Rome and Pescara) and Greece (0.9 between Agrinio and Skyros).

The south west / south east contrast between TX90 values evident in spring also strengthens into summer, and is evident for the western, central and eastern basins. Across Iberia there is a 4°C difference between very high south west TX90 values (Pegoes, 35°C) and high south east values (Valencia, 31°C), between the Greek stations of Ioannina (34°C) and Naxos (29.5°C) the difference is even greater.

The north / south contrast evident in spring precipitation indices develops further for summer (Fig. 3.7), providing a latitudinal dependence (Chapter 2.2.1) strong enough to remove the majority of regional differences in rainfall described for winter or spring. This contrast is more evident for PREC, PINT, PF90, and PX5D than other indices. Alpine summer rainfall produces fewer heavy events (1.6 days for PN90), but is generally more intense (PINT of 11.2 mm/day) than stations at similar latitudes (around 2.2 days and 7.5mm/day respectively). Otherwise there is little difference between northern Italian precipitation and rainfall in the south of France (PREC of around 2mm). North west Iberian stations behave much like those to the east (1.2mm PREC and 1.2 days PN90), although they possess slightly higher levels of rainfall (1.6mm PREC), and a greater number of heavy events (1.5 days PN90). Murcian stations are very dry (0.3mm), but not as dry as Seville (0.2mm) or Jerez de la Frontera (to the south west), or the south of Greece (0-0.1mm). The decrease in rainfall between spring and summer for Portugal, however, is dramatic (-1.5mm) as it drops to levels consistent with Murcia. In summer, central Portugal displays the longest dry periods (around 57 days) and lowest number of heavy events (0.52 days PN90) for the basin.

PCDD values are distributed in an inverse fashion (decreasing with latitude) upward of the southern coast of Iberia, Algeria, and the southern Balkans. For the most southern regions of the Mediterranean, dry days do not persist for nearly as long as those to the immediate north (17 days, as opposed to 36) although rainfall averages are lower (PREC near 0mm). For the same regions precipitation intensities (0.22mm/day) and persistent rainfall totals (7mm) are much lower than for central latitudes (around 8mm/day and 27mm). PQ90 values are anomalously high (71mm) for this southern

Iberian and Balkan region, and the difference from moderate to very high values is less a gradient (as for PREC, PF90 and PX5D indices), and more the boundary between two distinct areas. PINT values show similar, although less dramatic behaviour, with a north / south gradient and a distinct southern region of anomalously low values (0.2mm/day). For most of the southern area these values may be reflections of a largely arid summer regime under the influence of the sub-tropical jet and the African air mass (Barry and Chorley, 1998). This regime generally experiences very low levels of precipitation (under 1mm/day) and only very occasionally experiences very high levels of rainfall due to intense summer storms that may produce rain to the east of major mountain chains (Millán *et al.*, 2005).

Autumn

Autumn Mediterranean temperatures (Fig 3.8) are much lower than summer values, but are higher than those for spring (average temperature of 14.5°C). Although from spring to summer TX90 and TN10 temperatures increase by roughly the same value (8°C on average), from summer into autumn extreme high temperatures (TX90) show a much smaller decrease (average of 5°C) than extreme low temperatures (TN10 average decrease of 8°C). The range between northern and southern stations is larger than the range for either summer or spring (6.3°C for TAVG between Dar El Beida, 19.3°C, and Lazzaro, 13°C), particularly between high and low extremes (30°C between a southern TX90 of 30.6°C and a northern TN10 of 0.6°C). There is, however, a high level of similarity between the spatial distribution of temperature indices (TAVG, TMAX, TMIN, TN10, TX90) for both seasons. Generally the patterns described above for spring temperatures also hold for autumn.

The range between southern, low altitude, high TX90 values and northern, high altitude, low TN10 values is comparable to that for spring (36°C). However, a 9°C difference exists between Montseny Turo and Prat de Llobregat indices of temperature. The change from a smaller summer range is largely due to a decrease in low temperatures at high altitude. Low temperatures at height drop faster from summer into autumn than they rise from spring into summer, while low-lying high temperatures remain relatively high. In autumn frost days reappear over 300m but remain relatively scarce nearer sea level except on the northern boundary of the target region. Across

Iberia more stations experience frosts in autumn than in spring, but generally those stations experience a lower number of frost days over the season. For the eastern basin frost days are less common and last for shorter periods than those in spring.

Autumn HWDI values show differing behaviour for the eastern and western basins. Across Iberia the summer east coast low / west coast high contrast becomes less evident, showing a simple transition into the homogenous winter Iberian pattern, relatively low values (around 2.8 days) persist only for the extreme east and to the north of the peninsula. For the Balkans the summer contrast between east and west coasts increases, west coast values remain similar to those for summer (3.7 days), but east coast values are more consistent with winter warm spell lengths (3 days). This is also a form of transitory behaviour. For Italy, and the south east of France, although temperatures may not be as high, heatwaves last longer than in other seasons (a list of long and short lasting September central Mediterranean heatwaves is supplied by Colacino and Conte, 1995). Although TAVG, TMAX, TMIN, TN10, TX90, and to a lesser extent, TNFD indices show similar patterns in both autumn and spring, the distribution of HWDI values for autumn is unlike that for any other season. Despite these differences, much like the patterns evident for other indices in both autumn and spring, the autumn HWDI distribution largely demonstrates the seasonal change from a more zonal summer regime to a winter meridional circulation, as described in Chapter 2.

The change in circulation behaviour is also evident in precipitation indices (Fig. 3.9), as they largely return to a distribution similar to that described (above) for spring or (less so) winter, dependent on region. There is less of a latitudinal relationship for rainfall than summer or spring, and rainfall values are closer to winter levels than spring levels.

Rainfall is particularly high (5.9mm), intense (15mm/day), and persistent (PX5D of 151mm) for La Coruna and the north of Portugal, northern Spain and the south west of France (5.1mm, 12.6mm/day and 120mm for Biarritz), and to the south of the Alps (particularly Bosco, at 7.5mm, 21.9mm/day and 214mm), but there is little consistency with other stations of similar latitudes. Rainfall is low (PREC 1.5mm) and dry periods are long (PCDD 28 days) for Murcia, but extreme events are powerful (PQ90 31mm

and PINT 12.2mm/wd), if rare (PN90 1.1 days). There are few similarities between Murcia and central Portugal during autumn. Greek stations return to the spring wet west coast / dry east coast distribution for the majority of indices, and the north west / south east Aegean split for the remainder (3.3mm PREC. 22.8 days PCDD, 2 days PN90 for Agrinion in the west, 1mm, 42.5 days, and 0.85 days for Naxos in the south east).

In a manner more closely related to the winter distribution of indices than that for spring, extreme rainfall events occurring along the coasts of the Gulfs of Genoa and Lyons (including northern Italy, south eastern France, Catalonian Spain and the north of Corsica) are heavier (PQ90 around 34mm), more intense (PINT of 15mm/wd), longer lasting (PX5D around 120mm), and contribute more to the seasonal rainfall total (36% PF90) than events further in land. These values are generally only slightly higher than those for the west coast of Greece (by around 5mm, 0.5mm/wd, 25mm, and 4% respectively) and it seems likely that they are due in part to autumn cyclogenesis (Chapter 2.3.2).

Summary and Conclusions

The majority of interannual and spatial variation evident within the behaviour of extreme indices defined in the previous section is seasonal in nature, although more or less consistent variations exist between stations of varying altitude and latitude. During winter a distribution exists that suggests meridional (west to east) circulation. This shifts through spring into a zonal summer system (as detailed in Chapter 2.2). In many ways the autumn distribution of indices is very similar to that for spring, although temperature indices are closer to summer values and precipitation indices are slightly closer to winter values (Barry and Chorley, 1998).

However, although temperature indices display a strong seasonal cycle consistent between indices and largely consistent between regions, precipitation indices do not. Precipitation is generally low in summer, high in winter (as above), but winter rainfall values may be exceeded in either spring (northern stations, e.g. Turin, Paganella, Lyon, Clemont Ferrand) or autumn (e.g. Catalonia, the majority of southern Spain and Italy). Rainfall intensity (PINT) is one of only two indices that are at their highest everywhere simultaneously (during autumn), and at its lowest during summer

(with the exception of high values within the Gulf of Lyons and Genoa region). The other index is PN90, which is strongest during winter, and again experiences an almost basin-wide low during summer (excluding the northern stations of Turin, Paganella, Lyon, and Clemont Ferrand). Heavy rainfall (PQ90) may be heaviest in winter (north west Spain), summer (southern Spain and southern Greece) or autumn (everywhere else). Rainfall is most persistent (PX5D) during winter for eastern Greece and Portugal, but is otherwise at its height for autumn. Dry days persist for longest during summer for the majority of the basin, but last longer for southern Spain and southern Greece during autumn. PF90 is generally higher in autumn, then spring, but although the lowest values can be found south of 42°N during summer, stations to the north are as high or higher during summer months than in other seasons. It can be seen that there is little consistency in seasonal behaviour between indices of extreme rainfall, and that they are likely to be more dependent on circulatory factors, as detailed below.

Beyond precipitation seasonality, variations that have been expanded from detail in Chapter 2 to include indices of extremes in this section, are as follows:

- o In winter the majority of temperature indices (although not HWDI) are related to latitude, while precipitation indices show a more distinct latitudinal relation during summer (less so for PN90).
- o Temperature is also related to altitude, and extreme indices vary more with height than average values (particularly extremes of high temperature).
- o Stations near to coastlines are generally much warmer than those further in land during winter and mildly cooler in summer. This effect is particularly strong upon winter high temperatures (TX90) and frosts (TNFD).
- o Altitude has a negative effect upon precipitation (Agnew and Palutikof, 2000), but the location of stations with regard to mountain chains and coastlines is more important, and has an effect dependent upon the prevailing direction of circulation. The location of stations is particularly important near the coasts and mountains of Greece and for the south east and north west of Iberia.

o There is a mild west / east winter polarity evident for precipitation (PREC) that is also visible for the other indices of extreme rainfall. Generally the eastern basin receives more winter rainfall, shorter dry periods, and heavier extreme events than the western basin.

o Without the influence of very short periods of intense rainfall much of the southern part of the Mediterranean region (particularly South western Spain) would be completely arid (under southern influences) for the majority of the summer season.

More detailed conclusions, drawn directly from the data, are that:

o Stations at significant height (over 900m) exhibit less of a seasonal change in temperature indices than low-lying stations (particularly for TNFD).

o Beniston (2005) showed that unusually high temperatures in the Alps can persist for long periods in winter, and occasionally longer than they do in summer. This effect (illustrated by HWDI) also occurs across central and north eastern Spain, and for the Balkan mountain chain.

o For Iberian and Balkan summer, spring, and autumn, values, south western high temperatures (and their persistence), exceed those for the south east. This may be linked to south westerly flow produced by omega wave circulation, as detailed by Colacino and Conte (1995).

o North western Spain exhibits the greatest volume of rainfall, and some of the heaviest extreme events for the majority of the basin, across the greater proportion of indices. This behaviour peaks in winter and occurs for all seasons but summer, when Atlantic sourced flow is weaker than in other seasons.

o Other important regions for the generation of extreme rainfall include the western coast of Greece and the areas immediately surrounding the Gulfs of Genoa and Lyons. These areas coincide with the generation, regeneration, or tracks of Mediterranean cyclones (Table 2.2) and display long mean dry spell lengths but high precipitation intensities and PF90 values, suggesting infrequent but heavy cyclone generated rainfall.

o   By comparison the south east of the Aegean is generally dry during spring, summer, and autumn, and less prone to heavy rainfall. The behaviour of daily (non-extreme) precipitation in this region has been related to the frequency of cyclones that generate southerly or easterly flow (Maheras, 2006). In this section it can be seen that indices of extreme rainfall (PQ90, PINT, PCDD, PX5D) and average rainfall (PREC), possess similar distributions for the south eastern Aegean region.

3.4.3 Predictand inter-correlation

To demonstrate the relationships between the indices detailed above, all available values (all years, all stations) for each index have undergone (zero lag) testing for correlation (Section 3.3.4) with the values for all other indices, by season. Relationships that are both statistically significant and stable over the test period (Section 3.3.5) are detailed in Tables 3.5-3.8 as averages over the study region.

As all the predictands detailed above are derivatives of two different climate variables (temperature and precipitation) the most statistically significant inter-correlation exists within the group of temperature indices, and within the group of precipitation indices, rather than between them. Temperature (precipitation) indices generally correlate very well (significant at the 0.001 level) with TAVG (PREC) values, but less well with PREC (TAVG) values.

From season to season the inter-correlation between TAVG, TMAX, and TMIN is high and largely invariable (between 0.85 and 0.92), and although less high, correlations between these indices and HWDI (around 0.61) are just as consistent. Correlation results with average temperature (TAVG) are generally higher than those for TMAX or TMIN, which are greater than those for TX90 or TN10, which are generally higher than correlations with indices of persistence (HWDI and TNFD). However, relationships with TNFD are highly seasonally variable, and seem related to the number of frosts occurring. TNFD correlation values reach -0.86 with TMIN during

winter, and are mostly statistically insignificant during summer. Measures of extreme warmth (cold) display high levels of inter-correlation, and lower correlation values with measures of extreme cold (warmth). Further, during winter significant correlations exist at the 0.01 level between TX90 and TN10 (of 0.54), and between TNFD and HWDI (-0.61), but during other seasons correlations between extreme high and low temperatures are low or non-significant. During winter the majority of variance within the full temperature distribution is shared, which suggests that the same factors may influence high and low extremes, during summer this remains the case for the more central range of temperatures (TAVG, TMAX, TMIN), but is not the case for more extreme values (TX90, HWDI, TN10, and TNFD).

Values of correlation between PREC, PINT, PF90 and PN90 are also relatively invariant from season to season (between 0.74, and 0.80 respectively). Correlation values between PREC and the remaining rainfall indices (PQ90, PCDD, and PX5D) are consistently high (around 0.69, -0.58 and 0.77) for all seasons but summer (0.40, 0.29, and 0.83). Correlations between PX5D and PREC, and between PX5D and PCDD are the only statistical rainfall relationships that are greater in summer than in other seasons, and they display the largest precipitation correlation values for any season (0.83 and 0.81, respectively). The Mediterranean summer rainfall regime may be a result of long dry periods (on the order of weeks) broken by semi-persistent spells of heavy rainfall (several days in length). With the exception of summer dry days, precipitation correlation results with measures of amounts of rainfall (PX5D, PN90, PINT, and PQ90) are generally higher than for measures of rainfall frequency (PF90 and PCDD).

The correlation values for relationships between rainfall indices and temperature indices are highly dependent upon season. During winter, precipitation (PREC) has a negative relationship with both very warm (TX90, -0.63) and persistently cold (TNFD, -0.56) weather, as do extreme rainfall events (particularly PX5D and PN90). However, average temperatures (TAVG) and low temperatures (TMIN, TN10) are positively correlated with precipitation indices, and generally extremes of rainfall (PQ90, PX5D, PINT and PN90) display a consistent correlation (around 0.47) with temperature (TAVG). Moderate winter temperatures are the most conducive to large volumes of rainfall.

For spring / autumn the negative precipitation correlation with high temperatures (TMAX, TX90, and HWDI) is also evident, slightly lower for TX90 (-0.50) and higher for TMAX (-0.52 / -0.55), and the positive (PREC) relationship with low temperatures (TMIN and TN10) persists (0.44 and 0.65 / 0.55). Average temperatures (TAVG), however, display a negative correlation with rainfall indices, rather than the positive relationship for winter. Spring / autumn precipitation is linked to relatively (but not extremely) low temperatures. Relationships between temperature indices and extreme rainfall follow those for average rainfall with exceptions between autumn HWDI and PQ90 (0.58), and spring TX90 and PF90 (0.45). During autumn and spring there are aspects of extreme rainfall that are positively linked to high temperatures.

For summer, correlation values between temperature and rainfall are entirely statistically insignificant or negative (and around -0.53), with the exception of heatwave duration (HWDI) and the number of extreme rainfall events (PN90, 0.47). The strongest correlations exist between TMAX and PREC (-0.56), and TX90 and PCDD (0.57),

After averaging only stable and statistically significant correlation values across the basin a few relationships show values less than that required for statistical significance. These correlations must vary strongly from one part of the Mediterranean to another, and include:

- o Winter correlation between TMAX and PX5D (-0.09), and TNFD and PINT (-0.10).
- o Spring TNFD and PREC (0.08).
- o Summer correlations between PCDD and TMAX (0.18).
- o Autumn correlation between TNFD and PREC (-0.10).

These relationships are shown in Figure 3.10 and it can be seen that the relevant values in Tables 3.5-3.8 are the result of relatively few stable and statistically significant correlations.

3.4.4 Trends in climate extreme indices.

In order to assess whether or not Mediterranean climate extremes are changing, all climate indices have been assessed for trends using the Kendall's Tau method (Section 3.3.3). Only statistically significant trends (at the 0.05 level) resulting from the Kendall's Tau test are considered in this section. All values quoted below are changes per year.

Winter

Winter temperature trends (Fig 3.11) range between $+0.05°C$ yr^{-1} and $-0.07°C$ yr^{-1} TAVG, with positive changes occurring throughout the western Mediterranean basin, and negative changes occurring across the eastern basin. Average (significant) temperature trends for the west and east are $+0.04°C$ yr^{-1} and $-0.05°C$ yr^{-1} respectively, and $+0.1$ day yr^{-1} and -0.1 day yr^{-1} for heatwave days. For the majority of the central basin, from 12°E- 20°E, trends are insignificant. The polarised east / west temperature trend pattern is apparent for all indices of extreme temperature, although some variations upon the pattern exist, largely between indices of extreme warmth and cold, and between TNFD and all other indices. Although within significant regions TMIN, TMAX, TN10, and TX90 differences from TAVG trend values are small in most cases, positive western trends for TMAX and TX90 and negative eastern trends for TMIN and TN10 are slightly greater (marginally, and by $+0.01°C$ yr^{-1}, $-0.02°C$ yr^{-1} and $-0.03°C$ yr^{-1} respectively) than those for TAVG. Positive trends for TMAX, TX90 and HWDI are statistically significant for the majority of Iberia, the south of France, northern Italy, and Monte Scuro (southern Italy). Negative trends apparent in indices of extreme warmth are statistically significant for the south west of Greece. By comparison TMIN and TN10 only show statistically significant positive trends for Alcuescar (central Spain), northern Spain, southern France, and north west Italy, and negative trends for Alghero (in Sardinia), Agrinio, Kalamata, and Samos (all in Greece). Frost day (TNFD) trends largely reflect those for TMIN, although some positive (but small) trends exist within the Iberian peninsula. Values for TNFD range between -0.5 days yr^{-1} and $+0.3$ days yr^{-1} for the western and eastern basins.

Rainfall trends for the basin are largely statistically insignificant for all seasons, including winter (Fig. 3.12). Where they are statistically significant most winter precipitation trends are negative. During winter positive trends can only be found for PF90 (+0.09% yr^{-1}) and PINT (+0.05mm/wd yr^{-1}) in Alcantarilla (south east Spain), and for PINT (+0.1mm/wd yr^{-1}) in Prizzi (south west Italy). Negative trends occur:

- o Across Portugal for PREC (-0.17mm yr^{-1}), PINT (-0.14mm/wd yr^{-1}), PN90 (-0.08days yr^{-1}), and PX5D (-2.1mm yr^{-1}, the largest decrease for the basin),
- o For Sardinian PREC (-0.04mm yr^{-1}), PQ90 (-0.20mm yr^{-1}), PN90 (-0.08 days yr^{-1}), and PX5D (-0.70mm yr^{-1}),
- o Northern Italian PX5D (-0.51mm yr^{-1}),
- o And Greek PREC (-0.05mm yr^{-1}), PINT (-0.08mm/wd yr^{-1}), and PN90 (-0.05days yr^{-1}).

In addition Skiros (Greece) shows major negative trends for all rainfall indices (e.g. -0.05mm yr^{-1} PREC, -0.24mm yr^{-1} PQ90, -1.13mm yr^{-1} PX5D) except PCDD, which is positive (+0.43days yr^{-1}), as are the majority of PCDD trends for the Mediterranean (around +0.45days yr^{-1}). The Sardinian trend for PCDD is unusual as it is negative despite negative trends for all other precipitation indices at that location.

Spring

Spring temperature trends (Fig 3.13) are largely similar in pattern to those for winter. A polarity continues to exist between the warming western Mediterranean (+0.04°C yr^{-1}), and the cooling eastern Mediterranean (-0.04°C yr^{-1}). For TMIN and TN10, trend patterns are almost identical to those for winter, although both indices show a greater (more statistically significant) warming of low temperatures for the southern Iberian peninsula (e.g. +0.03°C yr^{-1} for Seville) and cooling of low temperatures in Greece (-0.09°C yr^{-1}). Extreme high temperatures (TMAX and TX90) show slightly greater magnitude trends (generally +0.01°C yr^{-1} - +0.03°C yr^{-1} over TAVG trends) but less statistically significant warming in the south of Iberia (e.g. +0.04°C yr^{-1} TMAX for Seville), more in the north of the western basin, and some

warming in the eastern Mediterranean (e.g. +0.04°C yr^{-1} for Samos), even where low temperatures show statistically significant cooling. In Greece spring TMAX cooling trends are negligible for all stations except Kythira and Ierapetra TMAX values (-0.03°C yr^{-1}). This decrease in the eastern negative temperature trend is also apparent in average temperatures (TAVG). Heatwave trends are as those for winter although with fewer statistically significant stations. A major difference between spring and winter HWDI trends is in Alicante, where HWDI and TX90 values are declining (-0.09 days yr^{-1} and -0.04°C yr^{-1}). The frost day pattern also follows that for winter, though with fewer statistically significant stations and a decrease in range of trend values (around +0.2 days yr^{-1} to -0.4 days yr^{-1}).

Spring precipitation trends (Fig. 3.14) show even fewer statistically significant stations than for winter. Rainfall trends are negative for multiple indices only for:

- Penhas Dourados and Santarem (Portugal) PREC (-0.06mm yr^{-1}, -0.02mm yr^{-1}), PINT (-0.09mm/wd yr^{-1}, -0.01mm/wd yr^{-1}), PN90 (-0.07 days yr^{-1}, -0.04 day yr^{-1}s) and PX5D (-1.1mm yr^{-1}, -0.02mm yr^{-1}),
- Vigo Peinador (north western Spain) PQ90 (-0.41mm yr^{-1}), PF90 (-0.6% yr^{-1}), PN90 (-0.08 days yr^{-1}), and PX5D (-2mm yr^{-1}),
- And Kozani (Greece) PREC (-0.06mm yr^{-1}), PQ90 (-0.19mm yr^{-1}), PN90 (-0.05 days yr^{-1}), and PX5D (-0.64mm yr^{-1}).

However, positive trends exist for south of France PQ90 (+0.19mm yr^{-1}), and PF90 (+0.2% yr^{-1}), and also PQ90 (+0.16mm yr^{-1}), PINT (+0.06mm/wd yr^{-1}), PF90 (+0.7% yr^{-1}), and PN90 (+0.05 days yr^{-1}) for Italy. Particularly consistent and significant positive trends exist for Rome.

Summer

Temperature trends for summer (Fig. 3.15) show warming across almost the entirety of the basin. Only the western coast of Greece maintains a regional cooling trend, which is evident for TAVG (-0.02°C yr^{-1}), TMIN (-0.03°C yr^{-1}), TN10 (-0.03°C yr^{-1}), and TX90 (-0.03°C yr^{-1}), Elsewhere in the basin, single stations show some element of isolated cooling:

- Ligonchio (northern Italy), -0.04°C yr^{-1} TMIN, TAVG, TX90, and TN10, -0.03°C yr^{-1} TMAX

- Alicante (south eastern Spain), -0.05°C yr^{-1} TMAX, and –0.06°C yr^{-1} TX90

- Alghero (Sardinia), -0.03°C yr^{-1} TN10

Otherwise the polarity between east and west is evident only as a differing degree of statistically significant warming trends, which are greatest towards the south of France (+0.04°C yr^{-1} TMAX, 0.05°C yr^{-1} TAVG, 0.07°C yr^{-1} TMIN, TN10 and TX90) and north western Italy (+0.03°C yr^{-1} TAVG, +0.07°C yr^{-1} TMAX and TX90), and weakest toward eastern Greece (around +0.01°C yr^{-1} for all indices). TNFD trends are largely statistically insignificant for summer, although negative TNFD trends occur for Paganella (-0.09 days yr^{-1}), Villameca (-0.01 days yr^{-1}) and Sabinanigo (-0.01 days yr^{-1}), both stations over 750m in height. HWDI values show a mild lengthening (+0.1 days yr^{-1}) across the majority of north eastern Spain, southern France, Corsica, Sardinia, and north western Italy.

Precipitation trends for summer (Fig. 3.16) are entirely statistically insignificant except for:

- Burgos (in northern Spain), -0.21mm yr^{-1}PQ90, -0.6% yr^{-1}PF90
- Logrono (also in northern Spain), +0.05mm/wd yr^{-1}PINT
- Southern Spain –0.37 days yr^{-1} PCDD and +0.14mm yr^{-1}PX5D
- Northern Italy +0.04mm yr^{-1}PREC, +0.46mm yr^{-1}PQ90, +0.23mm/wd yr^{-1}PINT, +1.0% PF90, +0.07 days yr^{-1}PN90, and +1.35mm yr^{-1}PX5D
- Greece +0.41mm yr^{-1}PQ90 (for Naxos), +1.7% yr^{-1}PQ90 (for Kalamata), and -0.02 days yr^{-1}PN90 (for Skyros)

Autumn

During autumn (Fig. 3.17) the eastern cooling trend reasserts itself for all indices except TMAX and TX90. For southern Greece TX90 warming is greater than for any other season (e.g. +0.06°C yr^{-1} for Naxos), however, there are also more statistically

significant cooling Greek TN10 trend values than for other seasons (e.g. -0.07°C yr^{-1} for Milos). TMIN and TN10 cooling are also evident for Alghero (Sardinia, -0.04°C yr^{-1} and -0.09°C yr^{-1}), Monteombraro (Italy, -0.02°C yr^{-1}, TN10 not statistically significant) and Pescara (Italy, -0.02°C yr^{-1} and -0.03°C yr^{-1}). Indices of extreme warmth show cooling for Rome (Italy, -0.03°C yr^{-1} TMAX, -0.08 days yr^{-1} HWDI), Kalamata (Greece, -0.05°C yr^{-1} TMAX) and Alicante (Spain, -0.02°C yr^{-1} TX90). Elsewhere all statistically significant values for indices show a warming trend. Most of the statistically significant warming trends occur:

- o To the north west (+0.02°C yr^{-1} TAVG, +0.03°C yr^{-1} TMIN, +0.04°C yr^{-1} TN10), north (+0.04°C yr^{-1} TMAX, +0.05°C yr^{-1} TAVG, +0.09°C yr^{-1} TMIN), and east (+0.03°C yr^{-1} TMIN and TAVG, +0.04°C yr^{-1} TMAX, +0.04°C yr^{-1} TX90) of Spain,

- o In the south of France (+0.02°C yr^{-1} TMAX and TX90, +0.03°C yr^{-1} TAVG and TN10, +0.04 yr^{-1} TMIN),

- o And the north east of Italy (+0.02°C yr^{-1} TAVG, +0.03°C yr^{-1} TMAX).

Rainfall trends (Fig 3.18) are statistically insignificant throughout the western basin except for negative trends, throughout the central basin except for positive trends, and are mixed for the eastern basin. Iberian trends are statistically significant for:

- o Penhas Dourados (Portugal, -0.6% yr^{-1} PF90, -1.6mm yr^{-1} PX5D),
- o Huesca (northern Spain, -0.05days yr^{-1} PN90)
- o Montseny Turo (north eastern Spain, -0.17mm/wd yr^{-1} PINT, -2.4mm yr^{-1} PX5D),
- o And south eastern Spain (-0.48mm yr^{-1} PQ90)

Statistically significant trends for Italy are largely positive and the same in both the north and the south (+0.02mm yr^{-1} PREC, +0.38mm yr^{-1} PQ90, +0.15mm/wd yr^{-1} PINT. +0.4% yr^{-1} PF90, +0.06 day yr^{-1} PN90, +1.4mm yr^{-1} PX5D). Statistically significant Greek rainfall trends are negative for the north (e.g. Kozani, -0.02mm yr^{-1} PREC, -0.19mm yr^{-1} PQ90, -0.7% yr^{-1} PF90, -0.06 days yr^{-1} PN90), and positive for the south (e.g. Milos +0.60mm yr^{-1} PX5D).

Summary

The most distinct result from testing for trends within the indices of extremes is that a contrast exists between a warming western basin, and a cooling eastern basin. This contrast in temperature behaviour has been previously shown for mean temperatures (Maheras *et al.*, 1999a), the range of daily temperatures (Brazdil *et al.* 1996), and in terms of cold-spell days (Klein-Tank *et al.* 2002). A summary of trends averaged for the eastern and western basins, for all indices of extreme temperature behaviour detailed above, is available in Table 3.9. The east /west temperature polarity is at its greatest during winter, particularly for indices of extreme warmth (TMAX and TX90), and weakest during summer, when large regions of the Balkan peninsula display a mild warming trend instead of a cooling trend. Summer indices display the largest and most significant positive trends in temperature, at their greatest in the north and north western basin, up to +0.14°C yr^{-1} for TAVG in Paganella. Eastern winter values display the greatest cooling for the basin, with values of -0.07°C yr^{-1} TAVG in Kalamata. Generally, indices of extreme high temperature show a greater trend than average temperatures (but with the same sign) by +/-0.01°C yr^{-1} to 0.02°C yr^{-1}. Low temperature (TMIN and TN10) trends generally display lower than TAVG cooling or warming trends during winter (-0.01°C yr^{-1} to -0.02°C yr^{-1}), creating an increased temperature range (Brunetti *et al.*, 2000a), but higher than average or maximum warming trends during autumn (by +0.01°C yr^{-1} to 0.04°C yr^{-1}) and summer (for southern France), resulting in a shrinking temperature range (Beniston *et al.*, 1994; Heino *et al.*, 1999). Trends for TNFD are small, but tend to follow TMIN trends during winter, when they are at their greatest. HWDI trends are also small, and tend to follow those for TX90 but show far fewer statistically significant values.

Precipitation trends are largely statistically insignificant for the majority of the basin (Klein-Tank and Können, 2003). The lack of statistically significant trends makes it difficult to assess changes in trend behaviour from season to season or from index to index. However, a few conclusions can still be drawn:

- o The majority of statistically significant trends in the western and eastern basin show a decline in rainfall on the order of -0.01mm yr^{-1} during summer and -0.03mm yr^{-1} during winter for most indices.

- o Italian rainfall displays an opposing trend (+0.01mm yr^{-1} to +0.02mm yr^{-1}) (Klein-Tank and Können, 2003), largely as a result of increasing extremes of rainfall (Brunetti *et al.*, 2000b, 2001a) and particularly for the northern region during spring and autumn.

- o However, for some indices, in small regions of Spain, (winter PF90 and PINT, summer PINT and PX5D), southern France (spring PQ90 and PF90), and Greece (summer PQ90) intense rainfall also shows a positive trend (see above).

3.4.5 Summary

In this section a set of climate indicators have been introduced to represent extreme behaviour in Mediterranean climatology (Section 3.4.1). These indices have then been tested for seasonal and spatial variation (Section 3.4.2), inter-correlation (Section 3.4.3), and trends (Section 3.4.4) to address the basic issues of patterns evident in the data, co-variance, and changes over time.

To return to the null-hypotheses stated at the end of Chapter 2 (2.5) it can now be seen that extreme events do not vary uniformly across the region (hypothesis 3), and that extremes of climate have changed over the last half-century (hypothesis 4). Furthermore, it can be seen that there is a strong seasonal component of change, likely driven by a shift from a zonal to a meridional general circulation (Chapter 2.1) as reflected in the spatial distribution of index values for each season. Summer and winter distributions show varying degrees of covariance between temperature indices such that during winter all indices respond with a high degree of shared variance, but during summer high (TMAX, TX90) and low (TMIN, TN10) indices share little variance. Differences between the covariance of precipitation indices from winter to summer are even greater, as results reflect the existence of two entirely separate regimes (Chapter 2.1), one of largely shared variance across all rainfall indices, and the other with variance shared only between extreme indices of persistence (PX5D and PCDD) and rainfall (PREC). Trends apparent in data also change from season to season such that during summer there are few statistically significant precipitation trends at all, whereas

there are more (mostly negative) trends during winter. Where temperatures are warming they show greater trends during summer, and where they are cooling those trends are greatest during winter for all indices except TN10 (greatest cooling in autumn). Where cooling is prevalent it is greatest for indices of extreme cold, and where warming is evident it is greatest for indices of extreme warmth (Table 3.9). This shows that extremes of temperature are varying in a different fashion to mean data.

Also evident are substantial regional differences. These variations are most evident between the north and south and east and west, but also occur for smaller regions. Latitude is important for both rainfall and temperature indices, but the degree of effect that latitude produces is dependent on season. Rainfall indices show a greater relationship with latitude during summer, and temperature indices during winter (Section 3.4.2). Further, temperature trends to the south of the region are mildly less statistically significant during summer than in winter. A similar relationship cannot be drawn for precipitation due to the lack of summer significance. Differences between the western, central, and eastern basins are also more evident for temperature than precipitation. The western basin is warming, whereas the eastern basin is largely cooling (except for during summer). The eastern basin is, however, on average (over the test period) warmer than the western basin for most indices of extreme temperature. For precipitation values, the eastern basin is also generally wetter than the western basin during winter. Trends in precipitation show that both the western and eastern basins are becoming drier, while the central basin largely shows a positive precipitation trend. In addition to the differences between east and west there can be substantial differences between indices of extremes for high and low altitudes, east and west coasts, and between northern and southern portions of the same coastline. In the latter two cases results generally occur in patterns that might be associated with a strong seasonal prevalence of cyclonic or anticyclonic flow (Section 3.4.2 and Chapter 2.3.2), and the greatest variations can be seen in frost day occurrence (TNFD), and for indices of heavy rainfall (PF90, PN90, and PINT). Particular sub regions that demonstrate individual seasonal characteristics, generated by these variations include:

- o   The northern Meditteranean,
- o   Central Portugal,
- o   The north west (Galicia) region of Spain,

o   The north east (Catalonia) region of Spain,

o   The south east (Murcia) region of Spain,

o   The north of Spain, south of France, and north west of Italy,

o   The coastlines surrounding the gulfs of Lyons and Genoa,

o   Southern Italy,

o   The west of the Balkan peninsula,

o   The west coasts of the eastern basin,

o   The east coasts of the eastern basin,

o   North western Greece,

o   South eastern Greece.

It can be seen that the characteristics of Mediterranean extreme climate are highly regional in nature, and change substantially from season to season.

3.5 Climate predictor variables

3.5.1 Desirable qualities in predictors

Table 3.10 lists the qualities that climatological predictors should satisfy. Having rejected components of variance (which form the principal component predictors detailed in the next Section) that contribute little in the way of variance or appear to be artefacts of the PCA methodology (Section 3.3.6), all the following indices (described in Section 3.5.2 and Table 3.11) embody qualities that are related directly to mass movement within the atmosphere, and are therefore physically meaningful. As all predictor indices are defined within a window of latitude and longitude centred on the target region, they are likely to affect the climate of the Mediterranean, and substantial volumes of literature suggest that climate indices such as those detailed here can be directly statistically linked to extremes of climate within the region (Chapter 2.4.3). Such predictor/predictand statistical relationships are further explored in Section 3.6, and trend behaviour is looked at in Sections 3.4.3 and 3.5.5. Temporal lagging has been taken into account where appropriate (i.e., for the SOI).

As discussed in Section 3.2.3, all the predictor data utilised in this study are considered homogenous, reliable (as determined by wide usage and review), are widely (freely) available, and persistent over a common study period (1958-2000). Although there are long and detailed series for some of the circulation indices used in this study, constructed from pressure data, and sometimes reconstructed from proxy data for longer periods, all of the indices used here have been interpolated or averaged from NCEP pressure grids. This maintains consistency between indices of circulation. Furthermore, the NCEP/NCAR Reanalysis data from which predictors are drawn exists on the same (2.5x2.5) grid as output from recent Global Circulation Models (e.g. HADCM3), over the same period, at scales of known high performance (Reid *et al.*, 2001), a factor that may aid future work.

Independence of predictors is a subject that is explored by the use of cross-correlation (Section 3.5.3 and 3.5.6). Stationarity of any given climatological relationship (rather than of any particular variable) is an issue currently under discussion within the international community (Schneider, 2000; Mann and Rutherford, 2002; Pauling *et al.*, 2003; Rutherford *et al.*, 2003; Hunt, 2004; Jones and Mann, 2004; Fowler, 2005). For the purposes of this study it is important only that relationships (i.e. the degree of covariance) between major climatic variables remain stationary, and not that the climate itself remains stationary. Although, probably due to external forcing (Hunt, 2004), the existence of global warming would imply that mean climate does not. In this study, as in the majority of climate modelling research concerned with recent centuries (Jones and Mann, 2004) rather than the distant past (Yin and Battisti, 2001), it is largely assumed that relationships such as those utilised here are stationary.

The one potential climatological predictor discussed within Chapter 2 that is not represented in the remainder of this study is the All India Rainfall Index. The AIRI is drawn from rainfall (a category C NCEP/NCAR reanalysis variable) rather than pressure (a category A NCEP/NCAR reanalysis variable) data, and does not currently exist on time scales comparable to the other indices used for this study (it is computed over a 5 month monsoon season). Further, the AIRI is correlated with Mediterranean sea level pressures (Section 2.2.3), a variable also considered as a predictor. Due to this combination of issues, the All India Rainfall Index was not used for quantative analysis.

3.5.2 Defining circulation predictor indices

To explore the relationships between indices of extremes and larger scale atmospheric circulation, the dynamics described in Chapter 2 also require indices. For a number of well-defined and discrete oscillations or pressure centres these indices are well documented, for others, less so. Most of the indices of circulation are calculated by characteristic pressure differences between points located inside 'centres of action', often areas of particularly persistent high or low pressure which drive circulation around them (Barry and Chorley, 1992). These points generally lie in between NCEP/NCAR reanalysis gridpoints, and the method used for construction of required time series is 16 point Bessel interpolation (Section 3.3.2). The indices of circulation (Table 3.11) that have been constructed by this method (e.g. the NAO, SOI, and MOI), or by areal averaging of gridded pressure data (e.g. the SHI, and NSCP), or other methods reliant on such data such as the calculation of easterly or westerly flow (e.g. the ABI and EBI), are:

The North Atlantic Oscillation Index (NAO)

The NAO has well documented teleconnections across Europe (see Chapter 2). As a potential driver of mean climate in the western Mediterranean its inclusion here is essential. Multiple formulations of the index exist using various northern and southern sites (Jones *et al.,* 1997). Ponta Delgada (Walker and Bliss, 1932; Rogers, 1984, Jones *et al.,* 1997) is generally favoured for the southern site, and averages of Icelandic stations for the northern site (Jones *et al*., 1997). However, depending on application the best positions for calculation of the NAO vary by season and region (Jones *et al*., 1997). For correlation with Iberian rainfall, slightly better results are achieved with Gibraltar as the southern site (Goodess and Jones, 2002). This study follows Goodess and Jones (2002), and utilises the Gibraltar (36.1°N, 5.3°W) / Reykjavik (65.0°N, 22.8°W) NAO index.

The Southern Oscillation Index (SOI)

As seen in Chapter 2, less work on Mediterranean teleconnections with the Southern Oscillation Index have been conducted than for the NAO, but a few studies point to a possible Mediterranean linkage, particularly in the eastern basin (Price *et al*.,

1998; Kadioglu *et al.*, 1999; Rodo and Comin, 2000; Rodo, 2001). The SOI is calculated as the normalised pressure difference between Darwin (12˚S, 131˚E) and Tahiti (17˚S, 149˚W) (Ropelewski and Jones, 1987) and is often considered one of the most important drivers of global climate. As informed by Van Oldenborgh *et al.*, (2000) this index has been used lagged by a season.

The Mediterranean Oscillation Index (MOI)

There is no index for the Mediterranean Oscillation currently in wide use. There are, however, two versions put forward in papers as discussed in Chapter 2 (Conte *et al.,* 1989; Palutikof *et al.*, 1996; Corte-Real *et al.*, 1998b; Piervitalli *et al.*, 1999; Palutikof *et al.*, 2003). Both of these are considered in the analysis at the end of this chapter, but only one is used for modelling purposes as they correlate highly with each other. The first index (MO1) is calculated by the normalised pressure difference between Algiers (36.4˚N, 3.1˚E) and Cairo (30.1˚N, 31.4˚E) (Palutikof *et al.*, 1996), the second (MO2) is the same, but for Gibraltar's North Front (36.1˚N, 5.3˚W) and Lod Airport in Israel (32.0˚N, 34.5˚E) (Palutikof *et al.*, 2003).

The North Sea Caspian Pattern Index (NSCP)

The North Sea Caspian Pattern is a more recent development than the MOI. The constructed version used here is calculated from the normalised 500hPa geopotential height difference between averages of North Sea (0˚E, 55˚N and 10˚E, 55˚N) and North Caspian (50˚E, 45˚N and 60˚E, 45˚N) centres of action. This is the same formulation used as Kutiel and Benaroch (2002) who selected these locations by use of linear correlation between pressure grid points and a GIS approach.

The Siberian High Index (SHI)

Calculated by Panagiatopoulos *et al.* (2005) as the area average of SLP over 40-65˚N, 80-120˚E for winter months (selected after examination of monthly maps of SLP back to 1871), this index describes the strength of the Siberian high pressure centre. As the Siberian centre of action is only evident for winter months, the SHI used here has been calculated for autumn, winter and spring, but not summer. This is an extension to the original Panagiatopoulos index, calculated only for winter.

The Atlantic Blocking Index (ABI)

Providing for a measure of jet stream influence (i.e. zonal vs. meridional flow) across the European region, the Atlantic Blocking Index (Pavan *et al.*, 2000; Pavan and Doblas-Reyes, 2000) is computed by summing the Tibaldi-Molteni (Tibaldi and Molteni, 1990) blocking index over the longitudes 80-20°W. The Tibaldi-Molteni blocking index is a measure of easterly frequency (days per month) between 40-60°N during periods of westerly flow above 60°N (more than 5ms^{-1}). Both easterly and westerly flow are then estimated from daily Geopotential heights (Z500). Shown to correlate with the NAO, this is the only index currently available which allows for the inclusion (although in an inverse fashion) of the influence of the jet stream in this study. The Tibaldi Molteni blocking index utilizes a southern (GHGS) and northern (GHGN) 500hPa geopotential height gradient:

$$GHGS = [\frac{Z(\phi_0) - Z(\phi_s)}{\phi_0 - \phi_s}]$$
$$GHGN = [\frac{Z(\phi_n) - Z(\phi_0)}{\phi_n - \phi_0}]$$

(3.32)

Where:

$$\phi_n = 80^oN + \delta, \phi_0 = 60^oN + \delta$$
$$\phi_s = 40^oN + \delta, \delta = -5^o, 0^o, 5^o$$

(3.33)

If:

$$GHGS > 0$$
And:
$$GHGN < -10m \,/\, deg \; latitude$$

(3.34)

For at least one value of Φ, at a given time, then that longitude is said to be blocked.

The European Blocking Index (EBI)

Also formulated by Pavan *et al.* (2000), the EBI is computed in the same way as the ABI but between the latitudes 10W and 50E. Together the EBI and the ABI indices help to characterise the blocking behaviour across the northern bound of the target region.

Between them the indices detailed above (summarised in Table 3.11, and with more detail in Chapter 2) characterise, or are affected by, the majority of coherent large-scale atmospheric circulation in the European region. Remaining atmospheric factors include Mediterranean cyclogenesis, travelling high pressure ridges, the Iberian thermal low, and local winds, all of which are features of regional-scale pressure distribution. Principle Component Analysis allows for the inclusion of these factors as spatial and seasonal changes in pressure and humidity, and the resulting PC predictors are detailed in Section 3.5.4.

3.5.3 Circulation predictor inter-correlation

Predictor indices have undergone the same correlation analysis used for predictands in Section 3.4.4. As detailed in Section 3.5.1 it is important that the majority of predictors do not possess significant and stable inter-correlations. Where correlations are statistically significant and stable, results between Circulation indices (Tables 3.12-3.15) show that:

- o The two Mediterranean Oscillation variants show highly significant (at the 0.001 level) inter-correlation for all seasons (0.79-0.92), strongest in winter, when they are particularly highly correlated with the NAO (0.90/0.83). The NAO is also highly correlated with the MO for autumn (0.60/0.58) and spring (0.58/0.65).

- o As detailed in Chapter 2.3.1, the NSCP and MO indices do not correlate particularly well (seasonal average of -0.05), and do not share the same correlation with the NAO. NSCP and NAO correlations are weak for both autumn (0.10) and spring (0.07). They cannot, therefore, be seen as entirely analogous (Kutiel and Benaroch 2002).

- o The European Blocking Index correlates highly with the NAO (-0.81) and with the MO (-0.73/-0.65) during autumn.

- o The Atlantic Blocking Index correlates well with the Mediterranean Oscillation (-0.50/-0.60) during autumn and the North Sea Caspian Pattern during summer (0.47).

o The SOI (lagged by a season) has no significant or stable correlation with any other predictor.

During winter and autumn it can then be seen that there are strong co-variance relationships between the North Atlantic Oscillation, the strength of blocking conditions over Europe, and a pressure oscillation across the Mediterranean. For spring the relationship between the Atlantic and Mediterranean oscillations is also in evidence, but for summer the only circulation predictors to show strong and stable relationships are between the North Sea Caspian Pattern and Atlantic Blocking. These results show that there are changes in regime from winter to summer for both predictands and Circulation predictors.

3.5.4 Trends in circulation predictor indices

As this study hypothesises a link between hemispheric scale circulation and Mediterranean climatology, and it can be seen that Mediterranean climate is changing (Section 3.4.4), it must be considered that circulation may also be changing with time. Table 3.16 shows Kendall's Tau (Section 3.3.3) calculated annual trends for all predictors (as normalised time series averaged by season) used in this study, and those that are statistically significant. Further, time series plots for each index are provided in Fig. 3.19-27 with linear trends for the entire period. Trend behaviour is summarised below:

o Of the circulation indices, the strongest statistically significant trend ($+0.04$ yr^{-1}) can be found for the North Atlantic Oscillation during winter (its strongest season), behaviour supported by Osborn (2004).

o The Mediterranean Oscillation is also strongest during winter (Chapter 2.2.3), when it displays a statistically significant positive trend ($+0.02$ yr^{-1}). The previous Section details a positive relationship between the NAO and MO indices. During the summer months both MO indices show a significant negative trend (-0.01 yr^{-1}).

- o The Siberian High index (Panagiatopoulos *et al.*, 2005) is the only index with statistically significant trends for both spring and autumn (+0.02 yr⁻¹).

- o European Blocking shows the second strongest statistically significant trend (-0.035 yr^{-1}), also for winter, and of a similar magnitude to the positive trend for the NAO (the two are highly correlated). European blocking also shows a positive trend for autumn (+0.01 yr^{-1}).

- o Atlantic blocking shows no significant trend and neither do the SOI or the NSCP indices.

During winter, the circulation influencing the western basin (Chapter 2.2.3) shows an increase in values for NAO and the MO. The two indices are strongly linked for that season (i.e. they correlate highly significantly, Section 3.5.3), so it is possible that the trend in one is responsible for the trend in the other. During summer, when the NAO possesses no significant trend, the MO is instead decreasing. The EBI also increases during a season when the NAO does not display a significant positive trend. As trends and correlation values are complimentary (negative correlation, similar magnitude but opposite sign trends) it is also feasible that an increase in NAO strength during winter is linked to a decrease in European blocking activity.

3.5.5 Defining PC predictor indices

Whereas circulation predictor indices can be constructed to characterise large-scale atmospheric movements by comparing distant values for large pressure fields, such an approach is not appropriate for smaller features (e.g. the Iberian thermal low), or for those where no indices or well defined centres of action exist (e.g. the influence of the subtropical jet on the southern Mediterranean during summer). For these factors a method that is capable of highlighting regional centres of atmospheric variance, without large volumes of data, is required. As previously described in Section 3.3.6 Principal Component Analysis produces such results when applied to regional atmospheric fields. Here the fields analysed with PCA are those for sea level pressure (SLP), geopotential height at the 500hPa level (Z500), and specific humidity at the

850hPa level (SHM), as detailed in Section 2.3.1. Conducting principal component analysis upon SLP and Z500 data for the Mediterranean domain is not new, but is an essential step for the construction of predictors for this study. A relatively wide domain (10-70ºN, -50-50ºE) has been selected to include potential influences to the south or east of the basin that are not reflected in other predictors. After the rejection of components (Section 3.3.6) the remaining PC predictors (Table 3.3) can be represented by loadings plots (Fig. 3.27-3.38), checked against previous studies (Table 2.4) and compared to the average field for the appropriate variable (Fig. 2.3-2.5) by season. A summary of components is available in Table 3.3.

Winter

The first principal component (PC) of winter sea level pressure contributes almost half (49%) of the variance of the seasonal field (Table 3.3) and the appropriate loadings map (Fig. 3.27) strongly resembles both the first mode of winter variance seen in Maheras and Kutiel (1999), and the winter dry SLP anomaly shown in Corte-Real *et al.* (1998a). These patterns show a very deep European depression that channels flow toward the Iberian peninsula, and is associated with dry conditions in Portugal. By contrast the second component (16% of total variance) resembles the rainy pattern shown in Corte-Real *et al.* (1998a), a strong north Atlantic depression extending into the north western Mediterranean that produces an intensified flow of moist air along a track associated with the Atlantic cyclones detailed in Chapter 2.3.2. The third winter SLP component (10% of variance) shows the Icelandic low shifted significantly southward, a pattern that creates moist south westerly flow toward the Iberian peninsula and frequent, intense, episodes of rainfall over Portugal (Zhang *et al.,* 1997). The pattern for component four (10% of variance) is also similar to a pattern in Zhang *et al.* (1997), showing an extended Icelandic low and a north European high associated with moderate rainfall conditions in the eastern Iberian peninsula.

The pattern shown for winter geopotential height PC1 (35% of total variance) closely resembles the first component of European winter Z500 found by Thompson and Wallace (1998), the mid-tropospheric signature of their Arctic Oscillation, and the first SLP component. Component two (19%) resembles the Eastern Atlantic pattern, as shown by Wallace and Gutzler (1981), Barnston and Livezey (1987), and Pavan *et al.*

(2000), and the second SLP component. The third component (16%) for winter Z500 is similar to the Atlantic/European blocking regime that occurs across the north east of the Mediterranean region (Pavan *et al.*, 2000), and the third principal component of winter Z500 shown by Wallace and Gutzler (1981). The fourth component (12%) shows Siberian blocking that varies in phase with central Atlantic variance (Corte Real *et al.,* 1995) and low pressures over the Mediterranean basin.

High variance components for specific humidity tend to reflect the flow conditions evident in components for sea level pressure. The first winter SHM component (33% of total variance) shows a strong tropical plume to the south east (Chapter 2.3.1) and a track of variance originating to the south west of Iberia that continues eastward through the basin, with highs to the south east of particularly mountainous regions. This track follows the southern edge of the SLP variance structure seen in SLP PC2. In a similar fashion the second SHM component (11% of variance) is consistent with structures evident in SLP PC3. Eastward Atlantic flow occurring in conjunction with African west coast variability, as seen here, has previously been observed by Jost *et al.* (2001). The third specific humidity component (9%) shows a variance structure centred on the Iberian peninsula that is consistent with a low pressure zone drawing moisture from the south west and north east (Chapter 2.3.2) in anti-phase with values for the eastern basin (Section 2.3.2). Component four (8%) shows a Mediterranean pattern almost inverted from SHM PC1, with a more developed centre to the east of the Atlas mountains and no shared variance with the tropics. The fifth, and sixth winter components contribute relatively low levels of variance (6% and 5%). Component five shows a pattern consistent with SLP PC4, and the clockwise movement of dry air from Turkey and the Middle East toward the eastern basin.

Spring

For spring, the first component of SLP variance (32% of total variance) is simply a weakened version of the first component for winter (a European depression). Similarly, component two (19%) reflects the second winter component (north Atlantic depression, Atlantic cyclones), although in spring the east Atlantic high pressure zone is stronger than the Siberian zone. Component three (16%) shows a strong resemblance to the third winter component, and component four (9%) to the fourth. The third

component, however, does show an additional, low pressure, feature over central Africa, extending toward the Middle East and Turkey. The fifth component of spring SLP variance (5% of total variance) shows a pressure low consistent with easterly conditions (most prevalent in May) over the British Isles (Barry and Chorley, 1998) and westerly conditions over central Iberia.

Geopotential height components for spring show little similarity to those for winter, except for the first component (20% of total variance). The loadings plot for spring Z500 PC1 is similar to the East Atlantic pattern evident in PC2 for winter, shifted toward the north east, and also a situation of strong Siberian blocking as shown by Corte Real *et al.* (1995). Similarities between first components for SLP and Z500 persist in spring. Spring component two (19%) also shows developed blocking, over north eastern Europe (Corte Real *et al.,* 1995). The third component of spring Z500 (16%) shows a North Atlantic Oscillation (Chapter 2.2.3) with shared variance between the southern centre of action and a European deep depression (Maheras and Kutiel, 1999). Spring PC4 (10%) displays a pattern that enhances flow toward the eastern coast of the Iberian peninsula, particularly to the north east (Serra *et al.,* 1999). Component five (9%) shows a relatively weak East Atlantic / West Russia pattern (Panagiatopolous *et al.*, 2005). As with winter SHM, components six and seven contribute little to the sum of variance explained (6% and 5%), and show only weak features. Component six shows an oscillation in variance between the central Atlantic and the Mediterranean Sea. Component seven displays a high pressure zone over Iberia and a large Asiatic low pressure zone to the east, this combination draws cold, northerly air across the Pyrenees and into the Mediterranean (Esteban *et al.,* 2005).

As for SLP, specific humidity plots show distinctive similarities to SHM plots for winter. Unlike SLP plots, each of the relevant loadings diagrams displays a strong shift in location for all features. The first component of SHM variance (41% of the total) shows a similar pattern to winter PC1, although the influences of central Africa and the Middle East have developed and moved to the north east. Component two (12%) displays a similar relationship to winter PC3, although the Iberian centre of variance evident for winter is not apparent here. The third component (6%) resembles the second winter component, but shifted toward the south west. Spring PC4 (5%) shows behaviour more consistent with winter PC5, although eastern Mediterranean

influence has moved south east and a centre of humidity variance has formed over north western Africa.

Summer

By comparison with winter and spring loadings, summer sea level pressure centres are weak. The first component of summer SLP (33% of variance explained) is entirely based upon continental pressure systems for Africa, the Middle East, central Europe, northern Europe, and Iceland, similar to PC3 for spring but without a discernible Atlantic system. Component two (16%) shows an expression of the NAO, weak during summer (Chapter 2.2.3), with an extension of the Azores high into northern Europe, similar to the East Atlantic pattern. The third component (11%) shows a pressure system associated with westerly conditions over northern Europe (Barry and Chorley, 1998). Components four and five (9% and 6%) strongly resemble weaker versions of the fourth and fifth components for spring. The fourth component is also shown in Maheras and Kutiel (1999), and shows a shallow depression to the west of Britain and a weak blocking high to the north of Europe.

For summer the first component of Z500 variance (24% of variance explained) shows great similarity to the first summer component of SLP, creating a zonal circulation and westerly flow over the majority of the basin (Maheras *et al.*, 2000). The second component (16%) displays a weakened east Atlantic pattern (see winter PC1) shifted toward northern Europe, with a developed centre of pressure variance over the Mediterranean basin and a developed icelandic low. Maheras *et al.* (2000) show a similar pattern and attribute the latter variance to a cut-off-low positioned over the Balkans. There are also similarities between the third component (14%) and PC3 for winter, although they are less pronounced. Component four (11%) shows the same structure as winter PC1, although it is much weaker. Component five (8%) produces a low pressure gradient over the Mediterranean basin (Maheras *et al.*, 2000), as does component six. The latter two components contribute little in the way of variance (6% and 5%), and show only minor influence over the Mediterranean basin.

By contrast each of the four components of specific humidity for summer show centres of action that are located in, or extend into, the Mediterranean basin. The first

summer SHM component (contributing the majority of total variance at 47%) clearly shows a tropical band of variance reaching into the eastern basin with a tropical plume, and into the western and central basins across the north western region of Africa. The second summer component shows the opposite behaviour (7%), with a slightly suppressed tropical band and dry air extended into the western basin from Africa, and into the eastern basin from the Middle East and Turkey. Component three (5%) shows the influence of the Asiatic system upon the eastern basin, and shared variance with the western basin. The fourth component (also 5%) shows a small humidity gradient across the majority of the basin, except for a Turkish centre of variance that creates a large gradient across eastern Greece.

Autumn

The first component of SLP for autumn (33% of total variance) shows a pattern similar to spring PC1 for SLP, and that given for autumn in Maheras *et al.* (1999). This distribution of centres represents the induction of cold continental air over the west central Mediterranean by a pressure high off the west coast of England. Autumn component two (17%) is very similar to component two for spring, although the northern pressure centre is shifted to the east and both the southern and eastern systems are weak. The third SLP component for autumn (12%) resembles the fourth component of winter SLP and PC 4 for spring, displaced northward by a centre of variance over central Africa, an anomaly pattern shown by Corte-Real *et al.* (1999a) and described as a Blocking-like anomaly. Autumn PC4 (10%) shows similarities to the third PC of spring variance and PC1 for summer, although an Atlantic system is apparent that acts in opposition to the European/African centres of variance. Component five (9%) is similar to component 5 for both summer and spring and component 3 for winter.

Geopotential height components, as for winter, show by far the greatest contribution to total variance from the first component (30%). The pattern evident in the loadings pattern for Z500 PC1 strongly resembles both SLP PC1 and the pattern given by Kutiel and Benaroch (2001) for the North Sea Caspian Pattern. The second component (17%) resembles that for winter, as do components three (12%) and four (9%). Components five (similar to spring PC5) and six contribute a small proportion of

total variance (6% and 5%) but both show a small gradient over the Mediterranean basin with centres of variance over the west and east respectively.

The autumn first and second component loadings for specific humidity are similar to those for summer. Autumn PC1 loadings (36% of total variance) show a developed tropical band and eastern Mediterranean plume, although no African extension into the western Mediterranean and a developed central basin centre of variance. Component two 12%) shows a more coherent north African / Middle Eastern band than for summer. The third component of autumn specific humidity variance (8%) shows behaviour similar to a hybrid of winter and spring PC2 loadings. Autumn PC4 shows little resemblance to any other pattern, contributes little additional variance (5%), and produces only a small humidity gradient across the target region.

3.5.6 PC predictor inter-correlation

In this Section the PC predictors defined above are tested for inter-correlation, as suggested in Section 3.5.1, and performed for Circulation predictors in Section 3.5.3. Stable and statistically significant results (Tables 3.12-3.15) show that:

- o Due to the orthogonality ensured by PCA (Section 3.3.6) components of a given field do not inter-correlate.
- o However, due to shared forcing (Chapter 2.3.1) SLP and Z500 components share similar loadings features (above) and do inter-correlate.
- o SLP and Z500 first components correlate significantly (0.001 level) for all seasons but summer. The correlation is greatest in winter (0.97), then autumn (0.88), and spring (0.64). Relevant loadings patterns (above) show little similarity between seasons and when linked by correlation represent shared variance between European depressions and large-scale high latitude circulation for winter (Arctic Oscillation) and spring (East Atlantic Pattern), and southerly flow and the NSCP during autumn.
- o The first component of SLP also correlates with the second component of Z500 for summer (0.31, significant at the 0.10 level), components with loadings that also demonstrate shared variance between European

depressions and the East Atlantic Pattern. This behaviour and set of loadings patterns is further evident for second components of SLP and Z500, which correlate significantly (0.001) for autumn (0.76) and winter (0.93), and the second component of Z500 correlated (significantly, 0.01 level) with the third component of SLP for summer (0.69).

o The second component of SLP correlates significantly with the third Z500 component for both summer (-0.57) and autumn (0.70), showing shared variance between components with loading patterns displaying blocking activity and European depressions.

o Third components of SLP and Z500 correlate significantly (0.001) only for autumn (0.75) when both components possess loadings patterns displaying extended Iceland low behaviour.

o For winter (0.85) and summer (-0.56) the third Z500 component correlates significantly (0.001 level) with the fourth SLP component. In both seasons loadings patterns demonstrate an extended/displaced Icelandic low and north European blocking, weaker in summer.

o During winter the third SLP component shows significant (0.001 level) correlation with the fourth Z500 component (0.81), relevant loadings patterns show north European variance shared with east Atlantic variance. This behaviour is also evident for autumn, the fourth Z500 component and the fifth SLP component are significantly correlated (0.57) and loadings show similar (though weaker) patterns.

o The fourth components of summer SLP and Z500 correlate (-0.66) significantly (0.001 level), and show linked loadings plots similar (but with much weaker centres of variance) to first component correlations for winter (see above).

o Specific humidity components show no significant and stable correlation with SLP and Z500 components for either summer or autumn.

o During winter only the fourth SHM component correlates significantly with SLP (PC1, -0.57) and Z500 (PC1, -0.56), and there are similarities between the loadings plots for each component.

o   For autumn there are also significant correlations between SHM PC1 and SLP PC1 (0.53), and between SHM PC3 and Z500 PC6 (0.47), in both cases the variance of humidity is consistent with the pressure distribution (and resultant flow) described above.

As for circulation indices, there are strong relationships between changes in pressure in the north Atlantic, across northern Europe and within the Mediterranean, stronger in winter and autumn than summer. During summer and autumn changes in SLP and Z500 variance across northern and southern Europe are also linked to centres of variance in humidity in the east and central basins.

3.5.7 Trends in PC predictor indices

As can be seen in Table 3.3 the first component of variance for each field and season explains a large proportion of total variance. For all seasons but autumn the PC scores for the first components of sea level pressure, geopotential height, and specific humidity also possess statistically significant trend behaviour (Table 3.16). Plots of PC score time series are shown in Fig. 3.39- 3.50.

For sea level pressure the components whose loadings show patterns associated with European depressions (DJF and MAM PC1, JJA PC3, Section 3.5.4 and Table 3.7) show a decline in variance scores, stronger in winter (-0.043) than spring (-0.026) or summer (-0.024). The components that show loadings patterns associated with developed continental systems (JJA PC1 and SON PC4) show an increase in variance (+0.051), as does MAM PC3 (+0.044), which possesses loadings consistent with an easterly shifted Icelandic low.

The first component scores of Geopotential height also   show significant negative trends for winter (-0.043) and spring (-0.038), with loadings patterns associated with the Arctic Oscillation and the East Atlantic pattern, and a positive trend for summer (+0.054). Lower variance components show significant trends only for spring and autumn. Trends in scores for the fifth spring (+0.043) and autumn (+0.026)

components (with similar loadings patterns) are both positive, as is the trend for spring component four (+0.022, north easterly flow over Iberia). Scores for the fourth autumn component, with a loadings pattern that resembles the NAO and Mediterranean low pressures also show a negative trend (-0.041).

Specific humidity first component scores all show a negative trend (including autumn). The loadings pattern associated with the first SHM component includes a tropical plume for all seasons and each season's trend is of a similar magnitude, slightly greater for winter and spring (-0.064, -0.064, -0.060, -0.057). Also displaying negative trends are scores for MAM PC2 and JJA PC4, neither of which show centres of variance located over the Mediterranean. The only specific humidity component that shows a (weak) positive trend in scores (+0.009) is the second summer component, the loadings for which show dry air incursions into the western and eastern Mediterranean basin.

3.5.8 Oscillation and PC predictor inter-correlation

Having tested both PC and Circulation predictors for inter-correlation, and having found similar behaviour evident in both sets, PC predictors have also been tested for correlation with Circulation predictors (Tables 3.12-3.15):

- o The NAO correlates significantly with many of the SLP and Z500 components that show strong north Atlantic variance loading patterns, particularly those that show a strong Icelandic low, and a European depression. Correlations are very high during winter (-0.87 for SLP PC1 and -0.90 for Z500 PC1), lower for spring (Z500 PC3, -0.68), autumn (-0.71 for SLP PC2, and -0.53 for Z500 PC3) and summer Z500 (-0.55 for PC5), and at their lowest (although still significant at the 0.10 level) for summer SLP (-0.44 for SLP PC2).
- o Winter SLP and Z500 first components (themselves inter-correlated) both show highly significant correlations with MO1 (-0.81), MO2 (-0.84/-0.83), and the EBI (0.81/0.86). These relationships are not evident

for other seasons except autumn, when the first components for SLP and Z500 both correlate significantly with MO2 (-0.51/-0.40), and Z500 PC1 correlates significantly with the EBI (-0.44).

o At a temporal lag of one season the SOI does not correlate significantly with any PC predictor.

o Components that correlate with the NAO do not significantly correlate with the NSCP or the ABI.

o The NSCP is significantly correlated with winter Z500 PC3 (-0.70) and SLP PC4 (-0.66) which are inter-correlated, spring Z500 PC5 (0.67) and PC1 (0.49), summer Z500 PC2 (0.80) and SLP PC1 (0.31), also inter-correlated, summer SLP PC3 (0.57), and autumn SLP PC3 (-0.60). None of these components correlate with any other Circulation predictor. Of these components most show a degree of Atlantic blocking (e.g. winter SLP PC4 and Z500 PC3), or strong north sea centres of variance (e.g. summer SLP PC3) in the relevant loadings plots.

o The SHI only correlates significantly with other predictors (-0.70 Z500 PC2, and -0.60 SHM1) for autumn. The relevant loadings patterns show a developed Siberian pressure centre and the appropriate moisture flow.

o Specific Humdities only possess Circulation index correlations to MO1 (-0.55, DJF SHM PC2), the EBI (-0.50, DJF SHM PC4), and the SHI (-0.60, SON SHM PC1) during winter and autumn.

o The ABI shows few significant correlations with other predictors other than the NSCP (Section 3.5.3). Significant correlations exist with components of SLP or Z500 that show some degree of Atlantic variance, most evident in Winter SLP PC4 (-0.53 correlation) and Z500 PC4 (0.69), but also in spring Z500 PC2 (0.65), summer SLP PC3 (0.57), and autumn Z500 PC2 (0.53).

o Where SLP components (winter PC4, summer PC3) correlate significantly with the ABI they also correlate with the NSCP. These correlations show matching signs and magnitudes of similar significance (e.g. -0.66 and -0.53, 0.57 and 0.57).

o For winter, where predictors show significant correlation with the EBI they also correlate with the NAO and/or MO indices (as above). For

spring this is the case for Z500 PC3, but not SLP PC2 (correlation of 0.71). The EBI correlates with no other predictor during summer.

Stable and significant inter-correlations between predictors are not common (less than 5% of possible correlations for winter, less than 3% for summer), but where predictors inter-correlate they tend to do so in groups of two or three. As seen in Section 3.5.3, there exists a winter circulation that produces strong links between the NAO, the Mediterranean Oscillation, European Blocking and principal components that show strong, high latitude and eastern Atlantic, centres of variance. During summer these links become less statistically significant, and instead a regime exists where the NSCP is linked to the ABI and complimentary variance distributions. These two regimes are statistically separate, and do not correlate significantly with each other during any season. The Siberian High index correlates with no other circulation predictor and only significantly varies with Z500 or SHM during autumn, suggesting that its influence over the domain is weak during other seasons.

3.6 Predictor / predictand correlations

As detailed in Section 3.5.1, predictors used for statistical modelling should display independence and strong statistical relationships with predictands. Independence between predictors has been tested, demonstrating that predictors are largely independent but inter-correlate in small groups indicative of seasonal circulation regimes. Trends have been tested for predictors and predictands such that relationships between them can be analysed in terms of both high and low frequency variability. High frequency relationships (i.e. correlations) between predictors and predictands are tested in this Section. Tables 3.18-3.21 provide summaries of stable and significant seasonal correlations. Where correlations are mentioned in the following summary, they are both stable and significant at the 0.10 level, and display trends consistent between predictors and predictands, unless stated otherwise.

In Chapter 2.2.3 a strong link between the NAO and mean temperature has been discussed. Here it can be seen that for TMAX and TX90, measures of extreme temperature, the NAO also shows good and widespread positive correlations for all

months but summer and autumn (e.g. +0.59 spring TX90 for over 20% of stations). These are largely based around northern Iberia and Italy, avoiding the south of the basin (Fig 3.51), a pattern also evident for mean temperature (Hurrell and Van Loon, 1997; Pozo-Vasquez *et al.*, 2001). Correlations are negative but unstable in the eastern basin. Although there are many significant correlations between NAO and precipitation indices (e.g. +0.59 winter PCDD average for over 10% of stations) found across the Mediterranean (mostly in the west) during winter (less during summer), very few of them are stable throughout the study period (Fig. 3.52).

Figure 3.51: Correlation between the NAO and TMAX indices, significant relationships (at the 0.05 level) are shown as rings, significant and stable relationships as filled circles.

In winter and autumn the MO gives particularly widespread and very high correlations with rainfall indices (Fig. 3.53), largely across Iberia and Italy. Significant and stable values are generally as high or higher than those for the NAO (e.g. +0.59 winter PCDD average for over 20% of stations), there are also often more stations that display such relationships for any given season, as detailed for mean data in Piervitalli *et al.* (1999).

Figure 3.52: Correlation between the NAO and PREC indices, significant relationships (at the 0.05 level) are shown as rings, significant and stable relationships as filled circles.

Figure 3.53: Correlation between MO2 and PCDD indices, significant relationships (at the 0.05 level) are shown as rings, significant and stable relationships as filled circles.

Although correlations for MO1 are often slightly higher than those for MO2 (e.g. winter, spring, and summer TMAX correlations of 0.61 and 0.58 respectively), they are generally evident across less of the basin, and for a smaller number of the predictands. Large numbers of stations with significant correlations can be found for TXAV and TX90 (over 20% of stations, negative correlation), PREC (over 20% during summer and autumn, positive), and PCDD (over 30% of stations during winter, negative).

The SOI (at a one season lag) correlates significantly (and displays a consistent trend) with indices of extreme rainfall in most seasons, but with a high proportion (over 10%) of (western basin) stations only during autumn (e.g. -0.49 autumn PREC for over 10% of the basin). Autumn SOI/rainfall correlations are negative, whereas correlations for other seasons are positive. Correlations are particularly significant for PF90 (+0.64 in winter, spring, and summer, -0.41 in autumn), and PN90 (+0.65 in winter, spring, and summer, -0.44 in autumn). During autumn the most significant correlations are with PCDD (+0.56).

The NSCP is one of the few indices that persistently (from season to season and for a number of temperature indices) shows very high correlations (average -0.68 with winter TAVG) in the eastern basin. This effect is not in evidence for spring, and is weaker during summer and autumn (average -0.51 with autumn TAVG) than for winter. Precipitation indices do not show such high correlations with NSCP in the eastern basin.

The SHI correlates with temperature (+0.62 TMIN, +0.48 TN10) and precipitation (+0.56 PREC) indices during winter, thus confirming Panagiatopolous *et al.* (2005), but also displays correlations (of the same magnitude and sign) during spring. Further, it is evident that extreme values show significant correlation (+0.50 with winter PQ90). Autumn indices show no such relationship.

ABI correlations exist for a greater proportion of stations during winter than any other season, when negative correlations with TMAX (-0.58, over 20% of stations) and TX90 (-0.56, also over 20%) are particularly widespread through eastern Iberia and western Greece (Fig 3.54). Winter relationships with other (magnitude, rather than

persistence) temperature indices are also spatially persistent. During winter the EBI displays a correlation pattern that is coherent across indices, negatively correlated with all measures of high temperature (e.g. -0.56 TMAX), positively correlated with all measures of low temperature (e.g. +0.43 TMIN), and positively correlated with all (positive) measures of rainfall (e.g. +0.67 PREC). This cross-index coherence degrades in other seasons, but does not disappear entirely.

Figure 3.54: Correlation between the ABI and TX90 indices, significant relationships (at the 0.05 level) are shown as rings, significant and stable relationships as filled circles.

Strong inter-correlations between higher components of the SLP and Z500 fields are detailed in the previous section. Predictor-predictand correlations for the higher components of Z500 and SLP thus show some similarities. Common behaviour is particularly prevalent for winter precipitation indices (e.g. +0.65 winter PREC with SLP PC1, +0.67 winter PREC with Z500 PC1). The higher components of SLP also show a greater number of correlations (i.e. stable and significant correlations at more stations) than other predictors. This disparity is less apparent for summer and autumn than winter or spring. Whereas Z500 and SLP components generally give a greater number of stable and significant correlations for temperature indices than for precipitation, SHM components often provide a greater number of high correlations with precipitation indices. Correlations with SHM components show (+0.01 to +0.10) higher correlations

for summer and spring, than for winter and autumn, but are largely seasonally invariant between winter and autumn (e.g. +0.44 PINT PC2 for both seasons), and summer and spring (e.g. +0.55 PINT PC2 for both seasons).

In addition to the relationships detailed above that persist from one season to the next, a particularly persistent relationship exists between TMIN and SHM PC3, which is evident for a large proportion of stations (over 20% of stations), with the same value (+0.58), for all seasons but autumn. The correlation between SLP and TMIN shows the same behaviour (but at -0.56 for over 30% of stations) for all seasons.

The detail provided above demonstrates that there are many significant and stable relationships between predictors and predictands. Over 63% (67%) of possible combinations between the predictors and predictands used in this study show at least one station with a stable and significant correlation for winter (summer), although only 15% (7%) show correlations for more than 10% of stations. Significant and stable correlations tend toward the regional, with small areas of the Mediterranean displaying high values.

In general, stable and significant correlations for TAVG are rarely the highest of the temperature correlations for any given predictor, showing that although strong relationships exist between Mediterranean circulation and mean temperature (as detailed in Chapter 2), indices of extreme temperature may display stronger links. This is particularly the case for high temperature indices with the NAO, MO and SLP components (e.g. SLP PC2), and low temperature indices with SLP and SHM components (e.g. SLP PC2 and SHM PC3). Frost days, however, do not provide significant relationships outside of winter. For that season, significant correlations for more than 10% of Mediterranean stations are found only with MO2 (0.52), the first two SLP components (-0.53, +0.55) and the third SHM component (-0.54), all of which show values lower than for mean temperature.

Average precipitation (PREC) frequently provides the greatest precipitation correlation for any given predictor (Chapter 2 provides detail on links between mean rainfall and circulation). Here it can be seen that extremes of rainfall are less related to

circulation than the mean. For any given predictor there are generally less significant and stable correlations with rainfall indices than temperature indices. PQ90, PINT and PF90, in particular, show few such relationships in any season.

The eastern Mediterranean displays more stations that correlate with the available predictors than the western or central basins only for the NSCP and SHM PC5 in winter, Z500 PC2 in summer, and the NSCP and Z500 PC2 in autumn. For the remainder of relationships correlations are either spatially consistent across the basin or more prevalent for the western basin.

Due to the very strong relationship (detailed in Section 3.5.3) between the two Mediterranean Oscillation indices, and the correlation behaviour detailed above (higher for MO1, but more spatially persistent for MO2), only MO2 (Section 3.5.2) will be used for the rest of this study.

3.7 Summary and conclusions

This chapter has built upon the available literature (Chapter 2) to introduce a data set that will be used for further study, to confirm a variety of trends and relationships across the Mediterranean within the mean of climate data, and to expand knowledge concerning those relationships to the extremes of climate data. The last of these three describes the contrast in heating and cooling of hot and cold extremes between the western and eastern Mediterranean basins, and the highly regional response to a seasonal shift between zonal and meridional circulation in extreme indices of precipitation. In addition inter-relationships between predictors and varying measures of extreme climate behaviour have also been assessed, providing new detail on the links between various circulatory phenomena (e.g. between the NAO, MO, and European blocking), that vary from season to season as part of a shifting regime.

To summarise findings new to this chapter:

o Heatwave durations during winter (winter warm spells) are greater at height than sea level for the majority of the Mediterranean basin, and longer (by over a day) for the western basin than the east.

o A noticeable contrast between west coast and east coast heatwave duration exists for spring, summer, and autumn, with west coast heatwaves longer by 1-1.5 days than east coast heatwaves. A contrast also exists between south west and south east TX90 values.

o Winter frosts are substantially more likely (on average an additional 30 days of frost in the season) for regions that are influenced by the Bora and Vardarac winds than nearby regions that are not.

o The coastal effect on mean temperature (Chapter 2) is stronger on high temperatures (TX90) and frosts (TNFD) than average temperatures.

o During winter substantial differences exist between all indices of rainfall for eastern (dry) and western (wet) coasts. For spring, summer, and to a lesser extent autumn, this contrast is instead north west (wet) / south east (dry).

o The contrast evident for precipitation is also apparent for indices of extreme high temperature, which of all the temperature indices show the most significant (negative) correlations with rainfall.

o During winter, spring, and autumn, the Mediterranean area most susceptible to both high levels of precipitation and heavy rainfall events is the north west of the Iberian peninsula. The area surrounding the Gulf of Genoa shows the most intense (PINT, PQ90, and PX5D) rainfall. However, the rest of the central and western basins receive less heavy rainfall than the western Balkan peninsula, and more than the south east of Greece.

o Rainfall intensity is higher for autumn than any other season for the entire basin.

o Although Mediterranean climate behaviour for autumn is more similar to summer than winter, the range of extreme values in autumn is larger than either season, or for spring. High temperatures remain high, and both low temperatures and extreme rainfall are closer to winter than spring levels.

o Extreme temperatures are increasing for the western basin and decreasing for the eastern basin, a polarity greatest during winter. During summer the eastern basin shows a mild warming across all indices.

o For the basin as a whole temperature ranges between extremes (TX90 and TN10) are increasing slightly in winter and decreasing substantially during summer and autumn. These changes are mostly driven by changes in extreme low temperatures.

o Extremes of temperature and rainfall generally show the same relationships to latitude evident for mean variables, and also display changes from season to season consistent with the change from a zonal to a meridional circulation.

o Furthermore, during winter, temperature extremes (TX90 and TN10, HWDI and TNFD) are highly inter-correlated, but this is not the case for summer. There is a similar shift in precipitation indices, with a greater inter-correlation between measures of persistent rainfall in summer, and heavy rainfall in winter.

o This seasonal shift is also the case for circulation predictor indices, which show a strong inter-correlation between the NAO, MO and EBI indices during autumn and winter, and between the NSCP and ABI indices during summer.

o The winter regime is largely dominated by increasing activity in the North Atlantic. The NAO, MO, and north atlantic centred principal components have positive trends, while the EBI index has a negative trend. Neither the NSCP, or ABI, show significant trends.

o Extreme temperature indices show generally higher significant correlations than for mean temperature for all the predictor indices used in this study.

o These two seasonal changes (in climate and circulation) are linked for extreme temperature and precipitation. During winter the NAO and extreme temperatures show highly significant (0.001 level) correlations and complimentary trends, as do the MO and extreme precipitation behaviour.

o These links are substantially less significant for the eastern basin and during summer.

From these results, and in response to the null hypotheses from the end of Chapter 2, it can then be shown that:

o Extreme events do not vary uniformly across the region.

o There are trends within extreme event data over the last half of the 20th century.

o Mean temperatures are not increasing across the entirety of the basin.

o Indices representative of the surface climate regime of the Mediterranean display covariance (a statistical relationship) with indices representative of hemispheric scale air masses and localized effects.

o These relationships are not constant across the basin, but do extend to the tail ends of the surface variable distributions.

o In some cases relationships are stronger in the tails than for mean data

With these results, the validity of a study concerning changing extremes of climate, and their causes, can be assured. It is with this conclusion that this study progresses to the modeling stage detailed in Chapter 4.

Table 3.1: Station summary. List of all climate data sites retained for analysis. Sources are credited as ARPA-SMR (Agenzua Regionale Protezione Ambientale – Servizio Meteo Regionale), FIC/KNMI (Fundación para la Investigación del Clima / Royal Netherlands Meteorological Institute), or WMO (World Meteorological Organization)

	Country	Name	Code	Latitude	Longitude	Elevation	Source
1	Algeria	Dar El Beida	603900	3672	325	25	WMO
2	Croatia	Zabreb	142360	4581	1596	157	FIC/KNMI
3	France	Blagnac	76300	4361	136	151	FIC/KNMI
4		Clermont-Ferrand	746000	4578	316	330	FIC/KNMI
5		Lyon-Bron	748000	4571	495	201	FIC/KNMI
6		Bordeaux	751000	4483	-70	61	FIC/KNMI
7		Agen	752400	4418	60	60	FIC/KNMI
8		Montelimar	757700	4458	473	74	FIC/KNMI
9		Embrun	759100	4456	650	876	FIC/KNMI
10		Biarritz	760200	4346	-153	71	FIC/KNMI
11		Tarbes	762100	4318	0	363	FIC/KNMI
12		Marignane	765000	4345	523	36	FIC/KNMI
13		Nice	769000	4365	720	10	FIC/KNMI
14		Bastia	779000	4255	948	12	FIC/KNMI
15		Marseille	999010	4330	538	75	FIC/KNMI
16	Greece	Thessaloniki	310	4062	2295	32	FIC/KNMI
17		Larissa	166480	3965	2245	74	FIC/KNMI
18		Alexandroupoli	310627	4085	2593	3	FIC/KNMI
19		Kozani	310632	4028	2183	626	FIC/KNMI
20		Ioannina	310642	3970	2082	484	FIC/KNMI
21		Mitilini	310667	3906	2660	5	FIC/KNMI
22		Agrinio	310672	3862	2138	25	FIC/KNMI
23		Skyros	310684	3890	2455	18	FIC/KNMI
24		Tripoli	310710	3753	2240	652	FIC/KNMI
25		Samos	310723	3770	2692	7	FIC/KNMI
26		Kalamata	310726	3706	2200	11	FIC/KNMI
27		Naxos	310732	3710	2538	10	FIC/KNMI
28		Milos	310738	3674	2448	183	FIC/KNMI
29		Kythira	310743	3613	2302	167	FIC/KNMI
30		Ierapetra	310756	3500	2573	0	FIC/KNMI
31	Italy	Paganella	16022	4609	1102	2125	ARPA-SMR
32		Torino/Bric. D. Croce	16061	4502	744	709	ARPA-SMR
33		Rimini/Miramare	16149	4402	1237	12	ARPA-SMR
34		Pisa/S.Giusto	16158	4341	1023	2	ARPA-SMR

Table 3.1: Continued.

35		Pescara	16230	4226	1412	10	ARPA-SMR
36		Roma Ciampano	16239	4147	1235	105	ARPA-SMR
37		Trevico	16263	4103	1514	1085	ARPA-SMR
38		Monte Scuro	16344	3920	1624	1710	ARPA-SMR
39		Prizzi	16434	3743	1326	1034	ARPA-SMR
40		Alghero/Fertillia	16520	4038	817	23	ARPA-SMR
41		Alfonsine	ALFONSI	4450	1203	7	FIC/KNMI
42		Bobbio	BOBBIO0	4476	936	270	FIC/KNMI
43		Bosco Centrale	BOSCO00	4444	1003	748	FIC/KNMI
44		Forli Centrale	FORLI00	4421	1203	34	FIC/KNMI
45		Lazzaro Alberoni	LAZZARO	4503	971	50	FIC/KNMI
46		Ligonchio	LIGONCH	4432	1035	928	FIC/KNMI
47		Monteombraro	MONTEOM	4438	1100	727	FIC/KNMI
48		Monzuno	MONZUNO	4426	1126	620	FIC/KNMI
49		Porretta Terme	PORRETT	4415	1098	349	FIC/KNMI
50	Portugal	Santarem	1320000	3924	-870	54	FIC/KNMI
51		Pegoes	1670000	3863	-865	64	FIC/KNMI
52		Alvega	2120000	3946	-804	51	FIC/KNMI
53		Mora	2260000	3893	-816	110	FIC/KNMI
54		Penhas Douradas	5680000	4041	-755	1380	FIC/KNMI
55		Portalegre	5710000	3928	-741	597	FIC/KNMI
56	Romania	Calarasi	154600	4420	2733	19	FIC/KNMI
57	Russia	Izmail	338890	4540	2879	30	FIC/KNMI
58	Serbia	Nis	133880	4333	2190	202	FIC/KNMI
59	Spain	Villameca	272800	4263	-607	978	FIC/KNMI
60		Alcuescar	441100	3917	-622	488	FIC/KNMI
61		La Coruna	800100	4337	-842	58	FIC/KNMI
62		Santander Centro	802300	4345	-382	64	FIC/KNMI
63		Bilbao Aeropuerto	802500	4328	-290	39	FIC/KNMI
64		Santiago Compostela	804200	4288	-842	364	FIC/KNMI
65		Vigo Peinador	804500	4222	-862	255	FIC/KNMI
66		Ponferrada	805300	4255	-660	534	FIC/KNMI
67		Leon	805500	4258	-563	916	FIC/KNMI
68		Burgos Villafria	807500	4235	-362	890	FIC/KNMI
69		Logroño Agoncillo	808400	4245	-232	352	FIC/KNMI
70		Huesca Monflorite	809400	4208	-32	541	FIC/KNMI
71		Zamora Observatorio	813000	4152	-573	656	FIC/KNMI
72		Soria Observatorio	814800	4177	-247	1082	FIC/KNMI
73		Daroca Observatorio	815700	4110	-140	779	FIC/KNMI
74		Reus Base Aerea	817500	4113	115	73	FIC/KNMI

Table 3.1: Continued.

75	Prat de Llobregat	818100	4128	207	6	FIC/KNMI
76	Montseny Turo	818200	4177	243	1706	FIC/KNMI
77	Salamanca 'Matacan	820200	4093	-548	790	FIC/KNMI
78	Valencia	828500	3947	-37	11	FIC/KNMI
79	Alicante Ciudad	835900	3837	-48	82	FIC/KNMI
80	Sevilla Aeropuerto	839100	3742	-590	26	FIC/KNMI
81	Alcantarilla	842900	3795	-122	85	FIC/KNMI
82	San Javier	843300	3778	-80	2	FIC/KNMI
83	Jerez De La Frontera	845100	3673	-605	27	FIC/KNMI
84	Sabiñanigo	946000	4252	-35	790	FIC/KNMI

Table 3.2: Categories of skill as they refer to significance levels of correlation (r)

Significance level	Description
>0.50	Negligible
>0.10	Low
0.10	Moderate
0.01	Good/Highly significant
<0.001	Very good / Very highly significant

Table 3.3: Summary of variance explained by retained principal components. Missing components have been rejected by the Scree test, italicized components are considered suspect as artefacts of orthogonality.

Variable	Season	Retained component variance explained							Total
		1	2	3	4	5	6	7	
SLP	DJF	0.49	0.16	*0.10*	*0.10*	-	-	-	0.85
	MAM	0.32	0.19	0.16	0.09	0.05	-	-	0.71
	JJA	0.33	0.16	0.11	0.09	0.06	-	-	0.75
	SON	0.33	*0.17*	0.12	0.10	*0.09*	-	-	0.81
Z500	DJF	0.35	0.19	0.16	*0.12*	-	-	-	0.82
	MAM	0.20	*0.19*	0.16	*0.10*	0.09	0.06	*0.05*	0.85
	JJA	0.24	0.16	0.14	0.11	0.08	*0.06*	*0.05*	0.84
	SON	0.30	0.17	0.12	0.09	0.06	*0.05*	-	0.79
SHM	DJF	0.33	0.11	0.09	0.08	0.06	0.05	-	0.72
	MAM	0.41	0.12	0.06	0.05	-	-	-	0.41
	JJA	0.47	0.07	0.05	0.05	-	-	-	0.64
	SON	0.36	0.12	0.08	0.05	-	-	-	0.61

Table 3.4: Summary of predictands used in analysis and models

Acronym	Full name	Units	Definition
TAVG	Average temperature	°C	Averaged daily temperature
TMIN	Minimum temperature	°C	Averaged daily minimum temp.
TMAX	Maximum temperature	°C	Averaged daily maximum temp.
TN10	Cold nights	°C	10th percentile of temp. distribution
TX90	Warm days	°C	90th percentile of temp. distribution
TNFD	Frost days	Days	No. of days for which min. temp. is below 0
TXHW	Heatwave duration	Days	Max. no. of consecutive days with temp. above 90th percentile.
PREC	Precipitation	mm	Averaged total daily precipitation
PQ90	Wet days	mm	90th percentile of prec. distribution
PINT	Rainfall intensity	mm/wet day	Amount of rain per day with more than 1mm prec.
PF90	Fraction of rainfall due to very wet days	%	Proportion of total rain from days with totals exceeding 90th percentile
PCDD	Consecutive dry days	Days	Max. no. of consecutive days with less than 1mm prec.
PN90	Number of days classed as wet	Days	No. of days exceeding 90th percentile
PX5D	5 day maximum rainfall	mm	Max. prec. over 5 days

Table 3.5: Average inter-correlation between predictands for winter (DJF) where relationships are both significant (0.10 level) and stable. Stable relationships are those that maintain a significant correlation for both 1960-1980 and 1980-2000.

	TAVG	TMIN	TMAX	TN10	TX90	TNFD	HWDI	PREC	PQ90	PINT	PF90	PCDD	PN90	PX5D
TAVG	1.00	0.91	0.87	0.78	0.72	-0.80	0.62	0.51	0.46	0.47	0.00	-0.51	0.47	0.49
TMIN		1.00	0.76	0.83	0.64	-0.86	0.60	0.57	0.43	0.32	0.48	-0.51	0.50	0.54
TMAX			1.00	0.66	0.77	-0.70	0.63	-0.24	-0.53		-0.55	-0.57	0.35	-0.09
TN10				1.00	0.54	-0.79	0.53	0.53				-0.54	0.52	0.39
TX90					1.00	-0.63	0.70	-0.63					-0.53	-0.51
TNFD						1.00	-0.61	-0.56	-0.48	-0.10		0.52	-0.47	-0.51
HWDI							1.00	-0.49		0.50	-0.17	0.39	-0.05	0.52
PREC								1.00	0.70	0.70	0.62	-0.60	0.78	0.75
PQ90									1.00	0.84	0.80	-0.45	0.83	0.72
PINT										1.00	0.74		0.76	0.76
PF90											1.00		0.85	0.71
PCDD												1.00	-0.50	-0.49
PN90													1.00	0.76
PX5D														1.00

Table 3.6: Average inter-correlation between predictands for spring (MAM) where relationships are both significant (0.10 level) and stable. Stable relationships are those that maintain a significant correlation for both 1960-1980 and 1980-2000.

	TAVG	TMIN	TMAX	TN10	TX90	TNFD	HWDI	PREC	PQ90	PINT	PF90	PCDD	PN90	PX5D
TAVG	1.00	0.87	0.92	0.65	0.67	-0.58	0.61	-0.52				0.51	-0.38	
TMIN		1.00	0.75	0.71	0.63	-0.66	0.55	0.44						
TMAX			1.00	0.59	0.72	-0.50	0.64	-0.52				0.53	-0.57	-0.53
TN10				1.00		-0.77		0.65						0.56
TX90					1.00	-0.17	0.62	-0.50	-0.46			0.55	-0.49	-0.39
TNFD						1.00		0.08						
HWDI							1.00	-0.57	0.58			0.52	-0.51	
PREC								1.00	0.66	0.69	0.64	-0.54	0.76	0.74
PQ90									1.00	0.83	0.80		0.84	0.68
PINT										1.00	0.74		0.75	0.75
PF90											1.00		0.86	0.69
PCDD												1.00		-0.49
PN90													1.00	0.71
PX5D														1.00

Table 3.7: Average inter-correlation between predictands for summer (JJA) where relationships are both significant (0.10 level) and stable. Stable relationships are those that maintain a significant correlation for both 1960-1980 and 1980-2000.

	TAVG	TMIN	TMAX	TN10	TX90	TNFD	HWDI	PREC	PQ90	PINT	PF90	PCDD	PN90	PX5D
TAVG	1.00	0.87	0.92	0.65	0.75		0.63	-0.54		-0.41	-0.48			-0.48
TMIN		1.00	0.73	0.75	0.65		0.59							
TMAX			1.00	0.60	0.81		0.65	-0.56		-0.45		0.18	-0.55	-0.50
TN10				1.00										
TX90					1.00		0.70	-0.50		-0.50		0.57	-0.42	-0.55
TNFD						1.00								
HWDI							1.00	-0.52		-0.43		0.53	0.47	-0.50
PREC								1.00	0.40	0.73	0.66	0.29	0.78	0.83
PQ90									1.00	0.69	0.64	-0.28	0.69	0.52
PINT										1.00	0.80	0.61	0.76	0.76
PF90											1.00	0.55	0.91	0.72
PCDD												1.00	-0.56	0.81
PN90													1.00	0.75
PX5D														1.00

Table 3.8: Average inter-correlation between predictands for autumn (SON) where relationships are both significant (0.10 level) and stable. Stable relationships are those that maintain a significant correlation for both 1960-1980 and 1980-2000.

	TAVG	TMIN	TMAX	TN10	TX90	TNFD	HWDI	PREC	PQ90	PINT	PF90	PCDD	PN90	PX5D
TAVG	1.00	0.85	0.89	0.60	0.60	-0.33	0.65	-0.45				0.51		
TMIN		1.00	0.74	0.66	0.57	-0.48	0.61							
TMAX			1.00	0.54	0.64	-0.20	0.68	-0.55			-0.46	0.58	-0.54	-0.49
TN10				1.00		-0.69	0.51	0.55			-0.01			0.59
TX90					1.00		0.59				0.45	0.52		
TNFD						1.00		-0.10						
HWDI							1.00	-0.54	-0.50			0.56		-0.55
PREC								1.00	0.70	0.73	0.62	-0.58	0.79	0.79
PQ90									1.00	0.83	0.80	-0.41	0.84	0.72
PINT										1.00	0.75	-0.39	0.77	0.79
PF90											1.00	0.37	0.87	0.72
PCDD												1.00	-0.48	-0.53
PN90													1.00	
PX5D													0.75	1.00

Table 3.9: Average significant temperature trends for the western and eastern basins. All trends are per year and in °C except TNFD and HWDI , both measured in days.

	West				East			
	DJF	MAM	JJA	SON	DJF	MAM	JJA	SON
TAVG	+0.03	+0.02	+0.03	+0.01	-0.03	-0.02	+0.02	-0.03
TMIN	+0.02	+0.02	+0.03	+0.02	-0.04	-0.03	+0.02	-0.02
TMAX	+0.03	+0.03	+0.03	+0.01	-0.04	-0.01	+0.03	-0.03
TN10	+0.03	+0.02	+0.03	+0.01	-0.02	-0.05	+0.01	-0.08
TX90	+0.03	+0.02	+0.04	+0.01	-0.05	+0.01	+0.04	+0.02
TNFD	-0.10	-0.05	-	-0.02	+0.25	+0.12	-0.01	+0.14
HWDI	+0.03	+0.03	+0.03	+0.02	-0.08	+0.01	+0.03	-0.09

Table 3.10: Desirable qualities in climatological predictors

- o Predictors should be physically meaningful.
- o Strong statistical relationships between predictors and predictands.
- o Trends of predictors and predictands should be related in addition to high frequency variability.
- o Ideally, relationships between predictors and predictands should remain constant over time (stationarity).
- o Predictors should exhibit independence, with minimal collinearity
- o Spatial and temporal lags between predictors and predictands should be taken into account where they might affect relationships.
- o Predictors should come from homogenous, reliable and widely available observational data sets.
- o Predictor time series must be as long as, or longer than, predictand series.
- o Predictor variables must be readily available from, and reliably reproduced by, GCM output.
- o Predictors should be calculated at a temporal and spatial scale appropriate to GCM best performance

Table 3.11: Summary of predictors used in analysis and models

Acronym	Full Name	Definition
SOI	South Atlantic Oscillation	Pressure difference between Tahiti (17˚S, 149˚W) and Darwin (12˚S, 131˚E)
NAO	North Atlantic Oscillation	Pressure difference between Reykjavik (65.0˚N, 22.8˚W) and Gibraltar (36.1˚N, 5.3˚W)
MO1	Mediterranean Oscillation 1	Pressure difference between Cairo (30.1˚N, 31.4˚E) and Algiers (36.4˚N, 3.1˚E)
MO2	Mediterranean Oscillation 2	Pressure difference between Gibraltar (36.1˚N, 5.3˚W) and Israel (32.0˚N, 34.5˚E)
NSCP	North Sea Caspian Pattern	Pressure difference between North Sea (over 0-10˚E, and 55˚N) and North Caspian (over 50-60˚E, and 45˚N)
SHI	Siberian High Index	Area averaged pressure across 40-65˚N, 80-120˚E
ABI	Atlantic Blocking Index	Frequency of easterly flow between 40-60˚N over 80-20˚W
EBI	European Blocking Index	As above over 10˚W-50˚E
Z500n	Nth principal component of geopotential height at the 500hpa level	Dimensional reduction of field variance across (10-70˚N, -50-70˚E)
SLPn	Nth principal component of sea level pressure	Dimensional reduction of field variance across (10-70˚N, -50-70˚E)
SHMn	Nth principal component of specific humidity	Dimensional reduction of field variance across (10-70˚N, -50-70˚E)